



## RESEARCH ARTICLE

10.1029/2023JA031317

# 3D GUMICS Simulations of Northward IMF Magnetotail Structure

### Key Points:

- Signatures consistent with magnetotail reconnection are observed in a simulation driven by northward interplanetary magnetic field conditions
- The simulation results in the production of a closed magnetotail structure and polar cap arcs
- The above structure occurs within a magnetotail that is highly twisted such that open lobe regions cross the equatorial plane

### Supporting Information:

Supporting Information may be found in the online version of this article.









### Correspondence to:

L. J. Fryer,  
ljf1e19@soton.ac.uk

### Citation:

Fryer, L. J., Fear, R. C., Gingell, I. L., Coxon, J. C., Palmroth, M., Hoilijoki, S., et al. (2023). 3D GUMICS simulations of northward IMF magnetotail structure. *Journal of Geophysical Research: Space Physics*, 128, e2023JA031317. <https://doi.org/10.1029/2023JA031317>

Received 17 JAN 2023  
Accepted 17 JUL 2023

L. J. Fryer<sup>1</sup> , R. C. Fear<sup>1</sup> , I. L. Gingell<sup>1</sup>, J. C. Coxon<sup>2</sup> , M. Palmroth<sup>3,4</sup> , S. Hoilijoki<sup>3</sup> , P. Janhunen<sup>3,4</sup> , A. Kullen<sup>5</sup> , and P. A. Cassak<sup>6</sup> 

<sup>1</sup>School of Physics Astronomy, University of Southampton, Southampton, UK, <sup>2</sup>Department of Physics, Northumbria University, Northumbria, UK, <sup>3</sup>Department of Physics, University of Helsinki, Helsinki, Finland, <sup>4</sup>Finnish Meteorological Institute, Helsinki, Finland, <sup>5</sup>School of Electrical Engineering and Computer Science, KTH Royal Institute of Technology, Stockholm, Sweden, <sup>6</sup>Department of Physics and Astronomy, West Virginia University, Morgantown, WV, USA

**Abstract** This study presents a re-evaluation of the Kullen and Janhunen (2004, <https://doi.org/10.5194/angeo-22-951-2004>) global northward interplanetary magnetic field (IMF) simulation, using the Grand Unified Magnetosphere–Ionosphere Coupling Simulation version 4 (GUMICS-4), a global MHD model. We investigate the dynamic coupling between northward IMF conditions and the Earth’s magnetotail and compare the results to observation-based mechanisms for the formation of transpolar arcs. The results of this study reveal that under northward IMF conditions (and northward IMF initialization), a large closed field line region forms in the magnetotail, with similarities to transpolar arc structures observed from spacecraft data. This interpretation is supported by the simultaneous increase of closed flux measured in the magnetotail. However, the reconnection configuration differs in several respects from previously theorized magnetotail structures that have been inferred from both observations and simulations results and associated with transpolar arcs. We observe that dawn–dusk lobe regions form as a result of high-latitude reconnection during the initialization stages, which later come into contact as the change in the IMF  $B_y$  component causes the magnetotail to twist. We conclude that in the GUMICS simulation, transpolar arc-like structures are formed as a result of reconnection in the magnetotail, rather than high-latitude reconnection or due to the mapping of the plasma sheet through a twisted magnetotail as interpreted from previous analysis of GUMICS simulations.

**Plain Language Summary** When the magnetic field associated with the solar wind is directed “northward,” the Earth’s aurora can adopt a formation where a “bar” of emission crosses the otherwise dim region that lies poleward of the usual auroral emissions. These phenomena are called “theta auroras” (due to their resemblance to the Greek letter), or “transpolar arcs,” and have been observed from spacecraft observing the auroral regions. As spacecraft cannot directly observe the global configuration of magnetic field lines within planetary magnetospheres, simulations can be useful to gain insight into the possible structures that occur during different solar wind conditions. We use a global simulation to model the interaction between the solar wind and the Earth’s magnetosphere (the region of space around our planet) and see that a large-scale field line structure can form during certain northward-directed magnetic field conditions. When we trace these field lines to the ionospheric boundary, we find that they resemble the global structures that have been observed for auroral arcs that stretch across the polar cap (also named theta aurora or transpolar arcs). We also note some key differences in their formation process from observational results.

## 1. Introduction

### 1.1. Northward IMF

The response of the Earth’s magnetosphere to the incoming interplanetary magnetic field (IMF) is a complex and dynamic process. This coupling has been extensively researched for a southward oriented IMF, yet configurations of the magnetotail during northward IMF are less well understood. During strongly northward IMF, signatures associated with dual lobe reconnection have been observed (Cowley, 1981, 1983; Crooker, 1992; Imber et al., 2006, 2007; Russell, 1972), similar to that first proposed by Dungey (1963). Imber et al. (2006) found dual lobe reconnection signatures to occur for clock angles within  $\pm 10^\circ$  of zero, though Lavraud et al. (2005, 2006) found that they occurred over a wider range of up to  $\pm 45^\circ$ . More commonly, the IMF contains a significant  $B_y$  component, hence resulting in single lobe reconnection. This can occur either in one hemisphere or in both hemispheres but with different interplanetary field lines, resulting in the stirring of flux around the magnetosphere

©2023. The Authors.

This is an open access article under the terms of the [Creative Commons Attribution License](https://creativecommons.org/licenses/by/4.0/), which permits use, distribution and reproduction in any medium, provided the original work is properly cited.

(Crooker, 1992; Gosling et al., 1991, 1996; Kessel et al., 1996; Reiff & Burch, 1985; Russell, 1972). These types of interactions can cause highly complex magnetotail configurations, resulting in the production of dawn–dusk lobes during times when the IMF clock angle is larger.

Two linked phenomena that are associated with northward IMF are the presence of hot plasma populations within the lobes and transpolar arcs (TPAs). TPAs are large-scale auroral forms that protrude into the polar cap, typically stretching from the nightside to the dayside, during northward IMF conditions (see polar cap arc review by Hosokawa et al. (2020)). Previous case studies and statistical studies have investigated the presence of hot plasma within the high-latitude lobes and found it coincident with the formation of TPAs in the high-latitude polar cap (Coxon et al., 2021; Fear et al., 2014; Fryer et al., 2021; Huang et al., 1987, 1989; Mailyan et al., 2015). The hot plasma observations by Fear et al. (2014) and Fryer et al. (2021) were best explained by a mechanism first proposed to explain the presence of TPAs (Milan et al., 2005, discussed below). The plasma properties in these studies exhibited features consistent with a population on closed field lines and showed a good correspondence between the times in which the spacecraft observed hot plasma populations and the intersection of their footprints with TPAs in the polar cap.

## 1.2. Transpolar Arc Mechanisms

Large-scale TPAs were first observed by Frank et al. (1982) and later named theta aurora (Frank et al., 1986; where “theta aurora” typically describe arcs which span across the entire polar cap). TPAs typically occur during northward IMF conditions (Frank et al., 1982, 1986; Gussenhoven, 1982; Kullen et al., 2002). They have been observed globally and can occur in both hemispheres simultaneously (Craven et al., 1991; Mizera et al., 1987); however, non-conjugate arcs have also been observed (Østgaard et al., 2003). The topology of TPAs has long been debated. There has been evidence in the literature of polar cap arcs originating on open field lines (Gussenhoven & Mullen, 1989; Hardy et al., 1982; Østgaard et al., 2003) and closed field lines (Craven et al., 1991; Frank et al., 1982, 1986; Milan et al., 2005). Other studies argue that both types of arc can occur simultaneously within the polar cap (Hosokawa et al., 2020; Reidy et al., 2018). More recent observational evidence suggests that large-scale TPAs are likely to form on closed field lines (Fear et al., 2014; Fryer et al., 2021). Hosokawa et al. (2020) and Fear (2021) also discussed the origin of TPAs in recent reviews of polar cap arcs and northward IMF dynamics, respectively.

There are multiple theories proposed to explain how these large-scale arcs form. TPA mechanisms were compared by Fear and Milan (2012a), who detailed the dependence of their formation location on IMF  $B_y$ , the physical driver (e.g., reconnection, twisting of magnetotail), the region in which the driver is located (e.g., magnetotail, magnetopause boundary), and the expected timescales of the response to the IMF. The subsequent motion of TPAs is also controlled by the IMF  $B_y$  component (Cumnock et al., 1997; Frank et al., 1986; Milan et al., 2005). Some TPA mechanisms are based on observational studies (Chang et al., 1998; Milan et al., 2005), while others have been developed from simulation and modeling results (Kullen, 2000; Kullen & Janhunen, 2004; Naehr & Toffoletto, 2004; Slinker et al., 2001; Tanaka et al., 2004). Simulation results all show slightly different topologies in the magnetotail; however, most have shown that TPA-like structures within MHD-based simulations can form only after a  $B_y$  sign change, which is a condition not required observationally as detailed in statistical studies by Fear and Milan (2012a) and Kullen et al. (2015).

Another large-scale phenomenon commonly associated with northward IMF and the presence of TPAs is “horse collar” auroras. Horse collar auroras are defined as regions within the polar cap that contain a significant area of particle precipitation on the dawn and dusk sides (Hones et al., 1989; Hosokawa et al., 2020). Low-latitude spacecraft reveals that these structures contain smaller Sun-aligned arcs (Zhu et al., 1996). More recent studies such as Milan et al. (2020) and Bower et al. (2022) have linked the presence of these structures to dual lobe reconnection during geomagnetically quiet northward IMF conditions. Tanaka et al. (2017) discussed the results of a northward IMF simulation with a steady IMF  $B_y$  component, in which horse collar auroras formed. Multiple small-scale auroral arcs formed, which were aligned along the oval edge. The authors argued that shear flows were responsible for such structures (similar to the mechanism suggested by Zhang et al. [2020]). Horse collar auroras can be present without the need for a  $B_y$  sign change but are not always associated with the presence of TPAs.

We aim to investigate within this paper the mechanisms that form TPAs within MHD simulations and consider why previous simulation results seem to require a  $B_y$  sign change to produce large-scale closed structures when it is not required observationally.

### 1.3. Kullen and Janhunen (2004)

In this study, we re-examine the northward IMF simulation presented by Kullen and Janhunen (2004) (hereinafter referred to as KJ04) and go on to compare the results to more recent studies that discuss possible TPA mechanisms. In the original study (KJ04), the Grand Unified Magnetosphere–Ionosphere Coupling Simulation version 4 (GUMICS-4) was used to simulate the magnetospheric response to a number of different northward IMF solar wind conditions and thus to investigate the connection between magnetotail twisting and polar cap arcs. The first four runs within their study (1a–1d) looked at the effect on the polar cap, the plasma sheet and surrounding magnetotail, during constant clock angle conditions, with a range of clock angles from  $10^\circ$  to  $100^\circ$ . The results of these runs showed little evidence of arcs protruding within the polar cap, consistent with the results of previous MHD simulations, which necessitated an IMF  $B_y$  sign change “trigger.” The two final simulation runs investigated by KJ04, runs “2a” and “2b,” looked at the effect of introducing a sign change in the  $B_y$  component of the IMF, through a rotation in the clock angle from  $-45^\circ$  to  $+45^\circ$ . In run 2a, this rotation was executed rapidly, whereas in run 2b, it was applied more slowly, over the course of an hour. In both runs, a large closed field line structure was observed after the  $B_y$  sign change moved past the nose of the dayside magnetopause. The authors commented on the formation of a “finger” of closed field lines in the tail, which bifurcated the lobes and mapped to a “bridge” of closed field lines in the polar cap (which they interpreted as an auroral arc).

KJ04 interpreted the large magnetotail structure (the “finger”) as a consequence of the relocation of the high-latitude reconnection site, coupled with a reversal of the twist in the magnetotail due to the reversal of the IMF  $B_y$  direction, thus combining two distinct elements of two previous models (Chang et al., 1998; Kullen, 2000). The plasma sheet twist was observed to be most severe in the far-tail regions and was argued to be consistent with the Kullen (2000) model, in which the authors argue that TPAs form due to the way in which the distant plasma sheet maps to the ionosphere when the near-tail and far-tail are twisted in opposite directions. Additionally, KJ04 interpreted their results as being consistent with the model proposed by Chang et al. (1998), where a “new” polar cap region forms as a result of a  $B_y$  sign change, trapping closed flux between the “new” and “old” polar cap regions. Both of these interpretations present theoretical problems which motivate our reexamination. As noted by Fear and Milan (2012a), the Chang et al. (1998) idea is premised on the assumption that the new magnetopause reconnection site (after the IMF  $B_y$  sign change) maps to a region that is equatorward of the open-closed boundary, which is physically impossible. Furthermore, in the original Kullen (2000) modeling, a modification of the Tsyganenko (1989) model is made in which two magnetotail regions, with opposite  $B_y$  components, are joined together through a transition region (with a length of  $10R_E$  or  $20R_E$ ). Kullen (2000) (later expanded upon by Kullen et al. [2002] in Figure 2b) interpret the plasma sheet field lines in the far-tail as connecting to lobe field lines in the near-tail, which then map to a TPA structure in the ionosphere. However, the lobe field lines are topologically open, whereas the far-tail plasma sheet is closed, and the TPA (in the ionosphere) was interpreted to be closed. Therefore, this interpretation essentially has the effect of connecting the distant closed field lines of the twisted plasma sheet to both open and closed topologies in the near-tail region. These theoretical obstacles, combined with subsequent observational and theoretical developments outlined below, provide motivation for a re-examination of the original KJ04 simulation runs and further discussion of the results.

### 1.4. Li et al. (2021)

A recent study by Li et al. (2021) used OMNI data to simulate two real northward IMF events and compared the outputs from two different MHD models, BATS-R-US and OpenGGCM. The main results from the study were that during northward IMF conditions, open field line regions formed, which were twisted such that they left the simulation domain in the opposite hemisphere to the mapped ionospheric footprint. Li et al. (2021) observed that the lobe regions underwent a rotation within both model runs and found that as a consequence, these regions could come into contact. The cause of the migration of these lobe field lines toward the central axis, and resultant reconnection, was speculated to be due to magnetic pressure pushing open field lines toward this central axis, where the magnetic pressure was thought to be low. They discussed how the varying IMF  $B_y$  conditions can affect the occurrence and rate of reconnection, and how they compare to observations of substorms but did not explicitly

discuss the possible link to global arcs and auroral features (although a more recent study by Li et al. [2022] discusses the model results in context to TPAs). Additionally, they found signatures of fast earthward flows which indicated reconnection was taking place. They found that this only occurred in one of the two models, despite running both models with the same initialization conditions and solar wind parameters. We see similarities and differences between our results and the conclusions from Li et al. (2021, 2022), which we make direct comparisons to throughout this paper.

### 1.5. Milan Mechanism

Milan et al. (2005) proposed a mechanism to explain how TPAs can form, based on a period of bursty night-side tail reconnection during northward IMF. The study used the flux inside the polar cap to measure the rate of reconnection associated with the flux closure in the magnetotail during a period of northward IMF (Tail Reconnection during IMF-Northward Nonstorm Intervals, or TRINNIs—Fear & Milan, 2012b; Grocott et al., 2003, 2004, 2005, 2007; Milan et al., 2005; Nowada et al., 2018). Milan et al. (2005) proposed that a period of dayside driving with a nonzero IMF  $B_y$  component causes open magnetotail magnetic field lines to have a nonzero  $B_y$  component. As a result of this introduced twist, two things happen when tail reconnection subsequently occurs. First, the newly closed field lines in the Northern and Southern Hemisphere can have significant azimuthal separation, such that when return convection occurs around the flanks to the dayside, one footprint would trail behind the other and have to convect faster to catch up with the leading footprint. This fast convection flow in one hemisphere is believed to cause the observations of fast azimuthal flows associated with TRINNIs as first proposed by Grocott et al. (2003, 2004). Second, Milan et al. (2005) then argued that as a consequence of the twisted tail, closed field lines in a local time sector straddling the noon–midnight meridian could become “stuck,” as these field lines cannot simply convect either dawn or duskward. They proposed that this resulted in the buildup of closed field lines, which Fear et al. (2015) referred to as a “wedge,” with the footprints of the wedge mapping into the polar cap (forming a TPA). Milan et al. (2005) suggested that the subsequent motions of TPAs were a result of the circulation of polar cap magnetic flux and plasma excited by high-latitude reconnection and hence detailed how the motion of a TPA is likely to be dependent on both the local time of the arc and the sign and magnitude of  $B_y$ . A more recent study by Milan et al. (2020) also discusses the use of pressure pulses during TPA events to determine the length that the closed field line wedge extends into the magnetotail and argued that in a particular case study, the closed field line wedge extended up to  $90R_E$  downtail. We will use this study to compare the length of similar structures in these simulation results to the estimates from the pressure pulse brightenings.

The Milan et al. (2005) model has had success in explaining the time delay in the dependence of TPAs (Fear & Milan, 2012a; Kullen et al., 2015), the formation location and its relation to the sign of the  $B_y$  component (Fear & Milan, 2012a), and the association with the ionospheric “TRINNI” flows indicating magnetic reconnection in a twisted tail (Fear & Milan, 2012b). Furthermore, the Milan et al. (2005) mechanism predicts that the “wedge” of closed field lines in the magnetotail that is conjugate to the TPA should be populated by plasma that is relatively hot and dense compared with the lobe. This plasma should be intermediate in character between the cold, rarefied lobe plasma and the hot, denser plasma sheet because the field lines forming the TPA initially contain lobe plasma but contract after being closed in the magnetotail, which will compress and heat the plasma (though not necessarily to the same degree as in the plasma sheet). This plasma population was shown to be present and consistent with a closed field line topology by Fear et al. (2014), and the temperature (and its spatial dependence) was shown to be consistent with this mechanism by Fryer et al. (2021) and Coxon et al. (2021). Therefore, in this study, we compare the output of the GUMICS model under varying northward IMF conditions with the characteristics that have been previously observed based on the Milan et al. (2005) closed field line model.

### 1.6. Motivation

Several simulation studies, such as KJ04, have sought to reproduce magnetospheric dynamics during northward IMF. However, these simulations appear unable to reproduce TPAs which are not linked to an IMF sign change, which constitute the majority of cases observationally (see Fear & Milan, 2012a; Kullen et al., 2015 and references therein). The interpretations of these simulation results also differ from interpretations of observation studies, as they are based on mechanisms that are premised on an IMF  $B_y$  sign change “trigger,” such as those developed by Newell et al. (1997), Chang et al. (1998), Kullen (2000), Kullen et al. (2002), and Cumnock (2005). It is clear that the results of simulations and observations relating to the formation of TPAs have shown incompatible

**Table 1**  
*Input Solar Wind Parameters*

Parameter	Value	Unit
Density ( $n$ )	7.3e+6	1/m <sup>3</sup>
Temperature ( $T$ )	100000	Kelvin (K)
Magnetic field X-GSM ( $B_x$ )	0	Tesla (T)
Magnetic field Y-GSM ( $B_y$ )	$-5 \times 10^{-9} \rightarrow 5 \times 10^{-9}$	Tesla (T)
Magnetic field Z-GSM ( $B_z$ )	$5 \times 10^{-9}$	Tesla (T)
Velocity X-GSM ( $V_x$ )	400,000	m/s
Velocity Y-GSM ( $V_y$ )	0	m/s
Velocity Z-GSM ( $V_z$ )	0	m/s

conclusions, and hence a re-examination of these simulation results is needed. In particular, we investigate whether the “wedge-like” structures, inferred by Milan et al. (2005) and observed in the magnetotail by Fear et al. (2014) and Fryer et al. (2021), are present in simulations and whether they form by similar mechanisms to those inferred observationally.

In this study, we will address these questions by re-evaluating the results of the run 2a first detailed by KJ04 and compare them to the observational mechanism proposed to explain the presence of TPAs (Milan et al., 2005). In Section 2, we outline the details of the GUMICS-4 model, and in Section 3, we discuss the setup of the simulation run. In Section 4, we describe the results from the simulation originally carried out by KJ04 and make a direct comparison to the results we found. We lastly compare the results to the TPA mechanism proposed by Milan et al. (2005), observational TPA properties, and other northward IMF simulation results (e.g., Li et al., 2021) in Section 5.

## 2. GUMICS-4 Model

GUMICS-4 is designed to model the complex interaction between the solar wind and the coupled magnetosphere-ionosphere system. This code has been evolved from GUMICS-1, originally modeling two dimensions in 1993 (Janhunen & Huuskonen, 1993), to the most recent version GUMICS-5 (a parallelized version of GUMICS-4 [Honkonen et al., 2022]). In this study, we use GUMICS-4 to be consistent with the results of Kullen and Janhunen (2004). GUMICS-4 uses a 3D compressible MHD magnetosphere and electrostatic ionosphere (Janhunen et al., 2012). The magnetosphere is modeled between  $-224R_E$  and  $+32R_E$  in the  $X$  direction, the point at which the solar wind is introduced, and extends to  $\pm 64R_E$  in both the  $Y$  and  $Z$  directions. The MHD magnetosphere and ionospheric model boundary is fixed at a geocentric distance of  $3.7R_E$ , where the two regions are coupled by propagating the density  $\rho$ , pressure  $P$ , velocity parallel to the magnetic field, and magnetic field vectors, across this boundary every 4 s. The maximum spatial resolution achievable within GUMICS-4 is  $0.25R_E$ ; however, this can vary depending on the location within the grid as GUMICS uses an adaptive grid method, prioritizing near Earth and tail regions (Janhunen et al., 2012). Further information about the capabilities and setup of GUMICS-4 is provided by Janhunen et al. (2012).

Reconnection in ideal MHD simulations, such as GUMICS, occurs due to numerical diffusion allowed by the discretized grid. Despite this, signatures commonly associated with magnetospheric reconnection have been observed in previous MHD models (e.g., Fedder et al., 1995, 2002; Laitinen et al., 2005; Li et al., 2021; Usadi et al., 1993; Walker et al., 1993). Additionally, measurements of total polar cap precipitation from GUMICS-4 have compared well to observational studies, implying that the typical global magnetospheric dynamics (such as the Dungey cycle and resulting convection) are present within MHD simulations (Palmroth et al., 2006).

Locating reconnection regions in 3D simulations can be challenging due to complex field line topologies. The methods used to locate 3D reconnection regions differ from techniques used for 2D simulations, which involve locating  $X$ -points (see reviews by Parnell & Haynes, 2010; Pontin, 2011; Priest, 2016), or locating saddle points of the flux function corresponding to  $X$ -point locations (as in Hoilijoki et al., 2017). Laitinen et al. (2005, 2006) found that GUMICS replicated well signatures of reconnection commonly seen in observations (e.g., strong plasma flow reversals within a thin current sheet) during strong southward-IMF orientations. The techniques described by Laitinen et al. (2005, 2006), to identify and quantify regions of possible reconnection, are used within this study to locate possible reconnection regions within the GUMICS during northward IMF conditions.

## 3. Simulation Run

In this study, we present a single GUMICS run in which the IMF was directed northward for the entirety of the simulation (as previously described by KJ04 in their run 2a). The GUMICS model takes a list of solar wind parameters (listed in Table 1) in 1 min intervals, which it introduces into the simulation at the upstream edge of the simulation box ( $X = 32R_E$ ). All solar wind parameters were kept constant for the entirety of the run, with the exception of the  $B_y$  component of the magnetic field, which has a linear transition from negative to positive over the duration of 2 min. This transition occurs 2 hr after the start of the simulation (clock angle =  $-45^\circ$  at

120 min, 0° at 121 min and 45° at 122 min). Additional parameters such as the epoch time and date are required for the simulation to run, as the Earth's dipole tilt is calculated from these parameters. We have chosen to define the run at 26 August 2000 04:00 UT as it coincides with a dipole tilt value of zero. All results detailed in this study were run with the highest resolution (adaptation depth of 5), resulting in the smallest grid size of  $0.25R_E$ . Auroral conductances are driven by solar irradiance and field-aligned electric currents, where the solar irradiance is calculated by the model based on the epoch start date. These values were chosen with the aim to emulate the results of run 2a by KJ04.

## 4. Results

In this section, we give a direct comparison between the results of the original run 2a presented by KJ04 and our version of this run. We go on to discuss how we define regions of “reconnection” and the resulting global configurations during this simulation run.

### 4.1. Comparison With Kullen and Janhunen (2004)

Figure 1 shows six panels from the simulation; the timestamps shown above each panel refer to the time since the IMF  $B_y$  sign change has passed the dayside magnetopause boundary (at the magnetopause nose); hence,  $t = 0$  is the time that the midpoint of the  $B_y$  sign change reaches the nose of the magnetopause (as previously defined by KJ04). Therefore, panels (a)–(f) represent the state of the magnetosphere at  $t = -8, 7, 22, 37, 52,$  and  $57$  min, respectively. The magnetic field lines within each of these panels are shown in orange. They have each been traced using the same starting points, at  $\sim 10R_E$  intervals down the  $X$  axis, and additionally in a spherical shell above  $60^\circ$  latitude (in  $10^\circ$  increments) and in  $45^\circ$  longitude increments around the ionospheric boundary (at a radius of  $3.7R_E$ ). Note that as a consequence, we choose to observe the change in topology at set locations within the modeled magnetosphere, rather than the propagation of the same magnetic field lines throughout the run. A movie of these figures (including the initialization period) can be seen in Supporting Information S1.

During the initialization of the simulation, the dipole magnetosphere interacts with the incoming northward-directed ( $-45^\circ$  clock angle) IMF through high-latitude reconnection with the initially dipolar nightside field lines (shown in the movie in the Supporting Information S1). Some of the IMF field lines reconnect with the (initially closed) nightside dipolar field lines in just one hemisphere (e.g., at  $t = -88$  min in the movie), which has the effect of opening dipolar field lines. Others go on to reconnect in the other hemisphere too (e.g., at  $t = -98$  min); this strips away the large region of closed field lines (dipole structure) on the nightside (Fear et al., 2015; and Figures 1d and 1e of Milan et al., 2022). After just over an hour, a steady state is reached, where the majority of the closed field lines in the magnetotail are now open and only a small closed region remains (Figure 1a). This initialization results in two relatively “new” regions of open field lines which are like conventional lobe field lines except that they are connected to the solar wind on opposite sides of the equatorial plane (i.e., the Northern Hemisphere “open” field lines leave the simulation domain through the southern side, and vice versa), as indicated by the top and bottom arrow in Figure 1a. It also results in a region of “older” downtail interplanetary field lines that have disconnected from the magnetosphere and are hence curved anti-sunward (i.e., form a reversed “C” shape), as a result of their previous connection to the closed, dipolar magnetosphere (central arrow in Figure 1a, compare again with Figure 1e of Milan et al. [2022], also see more detailed discussion in Section 4.2). Both types of field line are visible at  $t = -8$  min, where the ends of these field line populations appear to intersect the  $X$  axis between  $X = -50R_E$  and  $X = -100R_E$  downtail (Figure 1a). We can therefore see from this initial timestamp that the steady state for constant northward IMF at a  $-45^\circ$  clock angle within GUMICS appears to show that the magnetotail consists of open (i.e., connected to the ionosphere in one hemisphere) and disconnected tail field lines (which are connected to the solar wind in both directions, and which we continue to refer to more generally as downtail interplanetary field lines), with only a small closed field line region close to Earth remaining. This is similar to that of the textbook magnetosphere (Nishida, 2000), except for the connection of the lobe to the “wrong” hemisphere. This connection arises as a result of the simulation. It is not clear, from an observational point of view, how closely this resembles the real magnetosphere under northward IMF conditions (when the magnetotail's structure will be influenced by earlier periods of southward IMF and the pre-existing high-latitude field lines are open). However, we note that the structure in Figure 1a resembles that expected for reconnection with initially closed high-latitude field lines (Cowley, 1981, 1983; Crooker, 1992; Fuselier et al., 2015; Milan et al., 2022) and

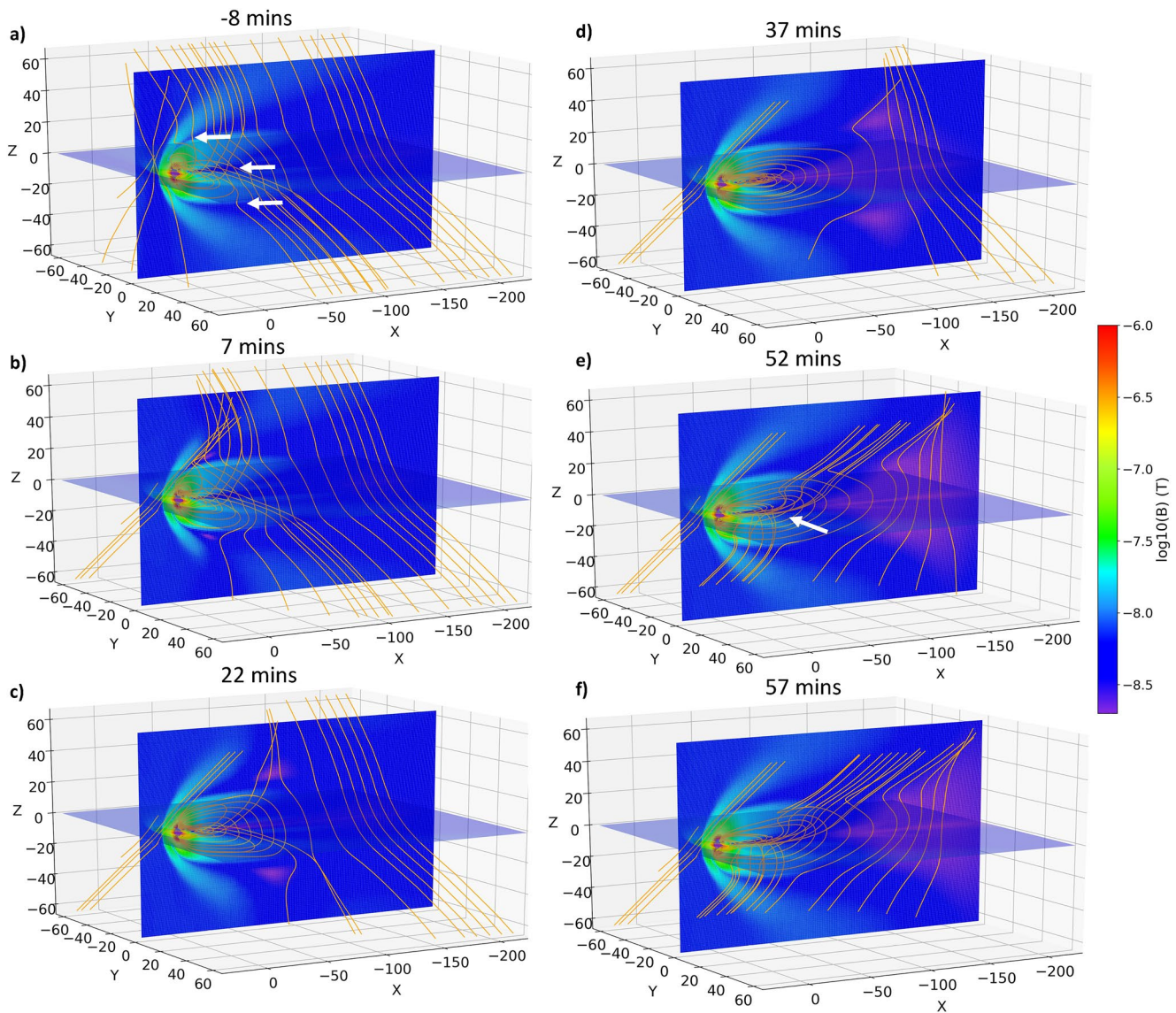


**Figure 1.** 3D plot of solar wind and magnetospheric field lines from the simulation run in Grand Unified Magnetosphere–Ionosphere Coupling Simulation (GUMICS). These panels correspond to the timestamps of –8, 7, 22, 37, 52, and 57 min since the IMF  $B_y$  sign change passed the nose of the magnetopause (the same times as shown in KJ04, their Figure 8). The background color indicates the log of the magnitude of the magnetic field strength in the  $X$ – $Y$  and  $X$ – $Z$  planes. The magnetic field lines within each of these panels are shown in orange.

also that observed in other simulations that are initialized with northward IMF conditions (e.g., Li et al., 2021, 2022 discussed below).

Figure 1b shows the simulation at  $t = 7$  min. The size of the closed field line region has increased both in length downtail ( $X$  axis) and in latitudinal extent ( $Z$  axis). Additionally, there is evidence that there has been penetration of the new  $B_y$  component into the near-Earth magnetotail lobes due to the rotation of the solar wind end of the most earthward open field lines, away from the original  $-45^\circ$  clock angle. (The  $B_y$  penetration during northward IMF is discussed in more detail by Browett et al. [2017] and Tenfjord et al. [2018] and references therein.) The downtail configuration of the magnetotail at this time remained relatively unchanged from the previous timestamp, which was prior to the introduction of the IMF  $B_y$  sign change region.

Figure 1c, at  $t = 22$  min (15 min later than the time shown in panel b), shows a completely different configuration. There is a significant portion of the magnetotail which is now closed (which we from this point on will refer to as the “wedge”), and we see that it extends to large distances downtail. The open field lines, which leave

the simulation box far downtail (which appear to intersect the grid boundary along  $X \approx 100R_E$ ), remain oriented inline with the original negatively directed  $B_y$  IMF component, with the nearest open field line again showing signs of rotation in the positive IMF  $B_y$  direction. The features discussed above from our Figures 1a–1c are also evident in Figure 8 of KJ04, and what we refer to as the “wedge” corresponds to the “finger” commented on in KJ04.

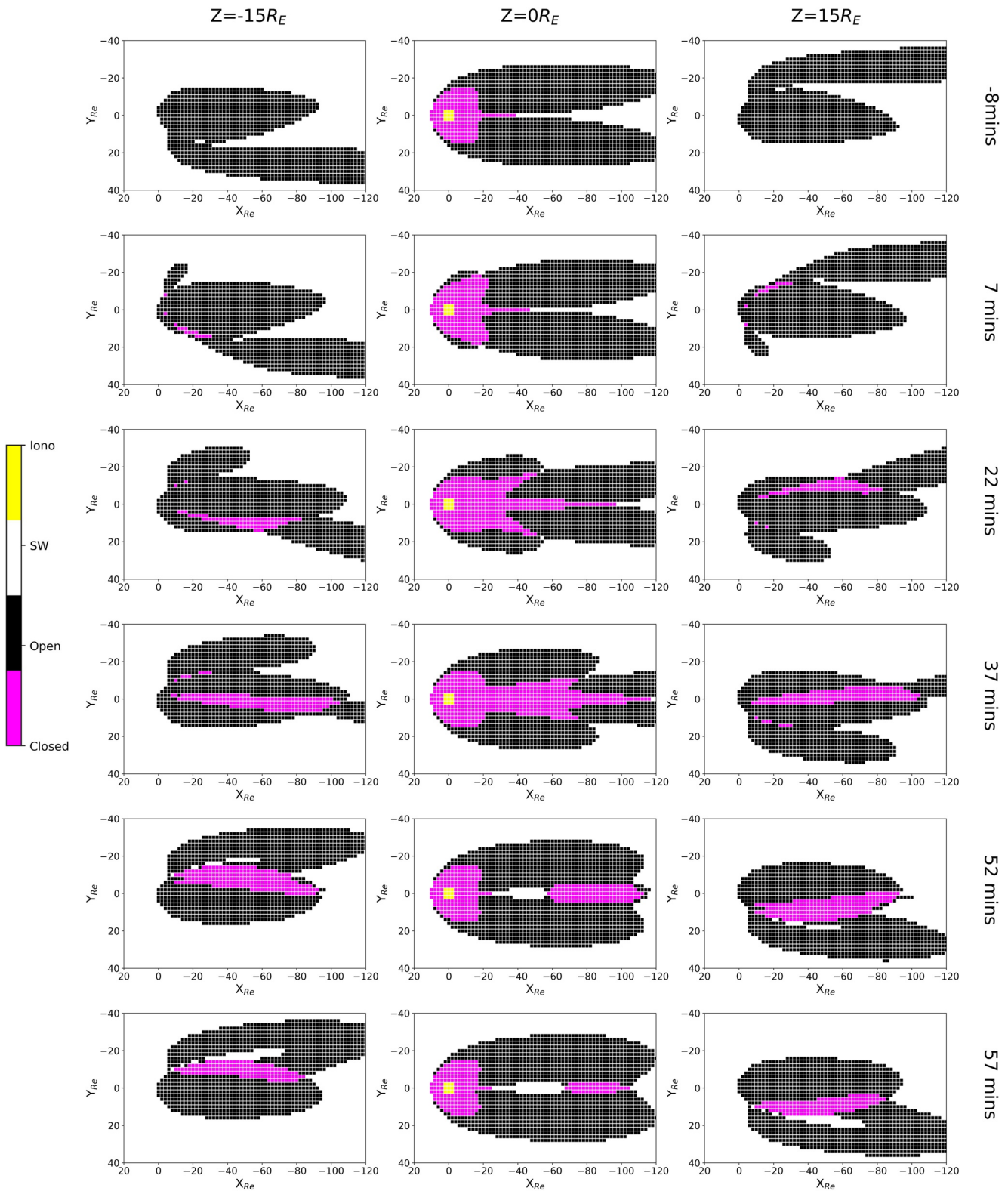
At  $t = 37$  min, the wedge appears to extend to its furthest length downtail, reaching  $-120R_E$  (further supported by the distances shown in Figure 2 which is discussed below). The newly oriented, positive IMF  $B_y$  component appears to have propagated into the distant tail region, which is evident in the change in orientation of the most earthward disconnected field line, and the change in orientation of the wedge itself from the previous timestamp. (We will further confirm these characteristics from Figure 2 which will be discussed below.) At  $t = 52$  min (Figure 1e), the wedge structure becomes more complex. The closed wedge now has the addition of embedded solar wind field lines which appear to thread through the center of the wedge (highlighted by a white arrow in Figure 1e, mimicking thread passing through the eye of a needle (Figure A1 in Appendix A provides additional views of this time stamp which confirms that the interplanetary population directly threads through the closed wedge structure). This appears to coincide with the start of the erosion of this closed wedge, which occurs as a result of high-latitude reconnection in both hemispheres “stripping away” the closed flux in a similar manner to the initialization. This is evident from the shape of the more earthward disconnected interplanetary field lines as they again form a backwards “C” shape, as a result of their earlier connection to the closed nightside field lines (see discussion above). This configuration indicates that high-latitude lobe reconnection with the closed wedge, converts magnetotail closed field lines to downtail IMF lines, oriented in the same direction as the “new” incoming solar wind. This configuration has been previously inferred using auroral data, where TPAs and cusp spots interacted during northward IMF conditions (Fear et al., 2015). It also bears strong similarities to “non-lobe” reconnection that has been observed with in situ observations (Fuselier et al., 2018; Lavraud et al., 2018).

Figure 1f shows that by  $t = 57$  min, these two processes (high- and low-latitude reconnection) appear to have almost completely eroded this wedge of closed flux, as only a small region of high-latitude field lines remains closed. The threading of flux through the center of this wedge is still present at this time, and we are left with the shell of closed field lines that have not yet been eroded by high-latitude lobe reconnection. It should be noted that the timings of the features in these last three timestamps differ slightly from the times at which they were observed by KJ04, though the features described above are all observed in their Figure 8. The wedge structure in our run appears to take longer to form as we observed no evidence of solar wind like field lines threading the wedge at  $t = 37$  min in our Figure 1d (this was observed by KJ04 in the top right panel of their Figure 8) and our structure appears to erode slower than that observed by KJ04 as we observe closed field lines associated with the original wedge at  $t = 57$  min in this run (Figure 1f), which are not present at the corresponding time observed by KJ04. In summary, the overall structures and configurations of field lines throughout this run have reproduced the global features observed by KJ04 and appear to deviate only by a small time lag on the order of minutes. We therefore will refer to the times as they appear within our simulation results going forward.

A second way to analyze this structure is to look at the topology of the field lines in the  $X$ – $Y$  planes, similar to that shown in Figure 7 of KJ04. We plot topologies of field line passing through the  $Z = 0, 15,$  and  $-15R_E$  slices in Figure 2. Here, the ionospheric boundary as well as open, closed, and solar wind field lines are plotted on a grid with a  $2R_E$  resolution in yellow, black, magenta, and white, respectively. Following KJ04, these plots have been cropped to a  $80 \times 140R_E$  grid which focuses on the region in which the wedge of closed field lines was observed in our Figure 1. Comparison with KJ04’s Figure 7 further confirms the similarity in the global simulations (as expected). By plotting the 2D  $X$ – $Y$  plane at different  $Z$ -values within the simulation, we can more clearly analyze the topological boundaries within the simulation. The times within this figure are the same times as shown within the 3D field line traces in Figure 1 and are indicated at the right-hand side of each row. The central and right-hand columns of this figure replicate what was first shown by KJ04 in Figure 7; however, we have also plotted the left-hand column showing the  $X$ – $Y$  plane at  $Z = -15R_E$ . This allows us to investigate the conjugacy between the two hemispheres in more detail, which will be discussed later.

Focusing first on the  $Z = 0$  plane (central column in Figure 2), at  $t = -8$  min, a thin and short ( $38R_E$ ) downtail extension of the closed field line region exists. At  $t = 7$  min, there is a small increase in the length of the closed field line region as it now extends to just past  $X = 45R_E$  (at  $Z = 0R_E$ ) with the width remaining initially no wider than the resolution of the grid ( $2R_E$ ), along the  $Y = 0R_E$  axis. As time progresses, this closed field line





**Figure 2.** 2D plots of the topology of the field lines in the  $X$ - $Y$  plane at three different  $Z$ -values of  $-15R_E$ ,  $0R_E$ , and  $15R_E$ . These panels correspond to the timestamps of  $t = -8, 7, 22, 37, 52,$  and  $57$  min since the IMF  $B_y$  sign change hit the nose of the magnetopause (the same times as shown in KJ04 Figure 7). The traces are shown at a  $2R_E$  resolution and the topologies indicated by colors, where solar wind (interplanetary field lines) are shown in white, open field lines in black, closed field lines in magenta and the ionospheric boundary is indicated in yellow.

region extends from  $\sim -40R_E$  to  $-120R_E$  downtail (between frames  $t = -7$  min to  $t = 37$  min), the longest length observed throughout the interval. This distance is slightly longer than an estimate of the closed downtail counterpart of a TPA from an observational study by Milan et al. (2020), who inferred that magnetotail distances could stretch to  $\sim -90R_E$  downtail. A slight increase in the width of this region can be observed as time progresses, with the width reaching a maximum of  $8R_E$ . Two secondary, smaller closed regions can be seen to extend tailward within the simulation, initially observed at  $t = 22$  min and located dawn and duskward of the  $Y = 0R_E$  axis. They form at  $Y = \pm 20R_E$  but appear to merge with the initial wedge of field lines and migrate toward the  $Y = 0R_E$  axis as time progresses (between  $t = 22$  min and  $t = 37$  min). By  $t = 52$  min, the main closed wedge appears to have separated from the near-Earth plasma sheet in the  $Z = 0R_E$  plane, as the region of closed field lines is only present between  $-60R_E$  and  $-120R_E$ . At first glance, this replicates what would be expected if a plasmoid had formed. However, by probing the  $Z = 15R_E$  and  $Z = -15R_E$  configurations, we find that this is not the case. This separation only occurs for small magnitudes of  $Z$  (i.e., close to the equatorial plane) as there is still a closed region extending earthward, and connecting to the near-Earth region, within these high  $Z$  planes. This is further confirmed by the field line traces shown in Figure 1e at this time, when the high-latitude closed field line structure spans this entire region, connecting to the Earth in the both Northern and Southern Hemispheres. This is contrary to a plasmoid, where the “pinching off” of the plasmoid would result in open field lines at higher latitudes between the plasmoid and the planet. The “separation” seen at  $Z = 0R_E$  at  $t = 52$  min is actually representing the “threading” of solar wind field lines initially observed in field lines plots (and discussed previously with reference to Figures 1e and A1). By  $t = 57$  min, this closed field line structure has reduced in size, no longer extending as far or as wide in the  $X$  or  $Y$  direction.

Studying the  $Z = -15R_E$  and  $Z = 15R_E$  planes (left and right columns of Figure 2), we gain information about the higher latitude field lines and also their orientation within the tail (which is difficult to quantify from field line plots alone). At  $t = -8$  min, we can see only the open field line regions in the lobes of the magnetosphere. Note that two “wings” of open flux occur on alternate sides of the central region in the northern and southern planes; these occur as the incoming solar wind has an initial clock angle of  $-45^\circ$ . Seven minutes after the  $B_y$  sign change region hits the dayside magnetopause, the closed field line region emerges in the  $\pm 15R_E$  planes. We note that interestingly, it appears on alternate sides of the magnetotail in the two hemispheres. Between  $t = 7$  min and  $t = 37$  min, these conjugate closed regions grow in both length and width, reaching just past  $-100R_E$  downtail. The location of this closed field line region in both hemispheres moves with time as we see a migration of the closed field lines in the dawn and dusk side toward smaller  $|Y|$  values, hence toward the central axis. This migration continues such that the position of the wedge at high  $Z$ -values moves to the opposite sides of the magnetosphere (i.e., opposite values of  $Y$ ), indicating that the wedge rotated through the midnight meridian between  $t = 37$  min and  $t = 52$  min. The position of the closed field lines along this alternate side is maintained throughout the rest of the simulation run.

The locations of the closed wedge and open field line regions compare well with the formation discussed by KJ04, though as we discuss below, our interpretation differs. The main observational differences occur in the later times of the simulation, as discussed above in the context of Figure 1. From  $t = 37$  min, we observe a delayed decay of the structure compared with that observed by KJ04 and a slightly longer closed field line region. We speculate that the most likely cause for this is a difference in grid resolution, as previous studies such as that by Gombosi et al. (1998) have shown that the length of the closed field line region can be related to the minimum grid resolution in MHD simulations during northward IMF. Despite this, the tailward extent of the wedge, which reaches a maximum downtail distance of  $\sim 120R_E$ , compared well with recent estimates of TPA downtail distances as discussed by Milan et al. (2020).

The overall global dynamics observed within our simulation results were similar to those presented by KJ04 and hence we do not believe the small-scale differences will affect the overall interpretation of this simulation.

#### 4.2. Search for Reconnection

From the initial results of the simulation, it appears qualitatively that there was an increase in closed flux measured within the magnetotail during the mid-stages of this simulation (based on the observations in Figures 1 and 2). To test this, we quantitatively measure the amount of closed flux threading the 2D  $X$ - $Y$ -GSM plane at  $Z = 0R_E$ , at each time interval shown in Figure 2. To do this, we calculate the flux mapping through each cell that is indicated as closed in the central column of Figure 2 (i.e., the  $Z = 0$  plane), by multiplying the component

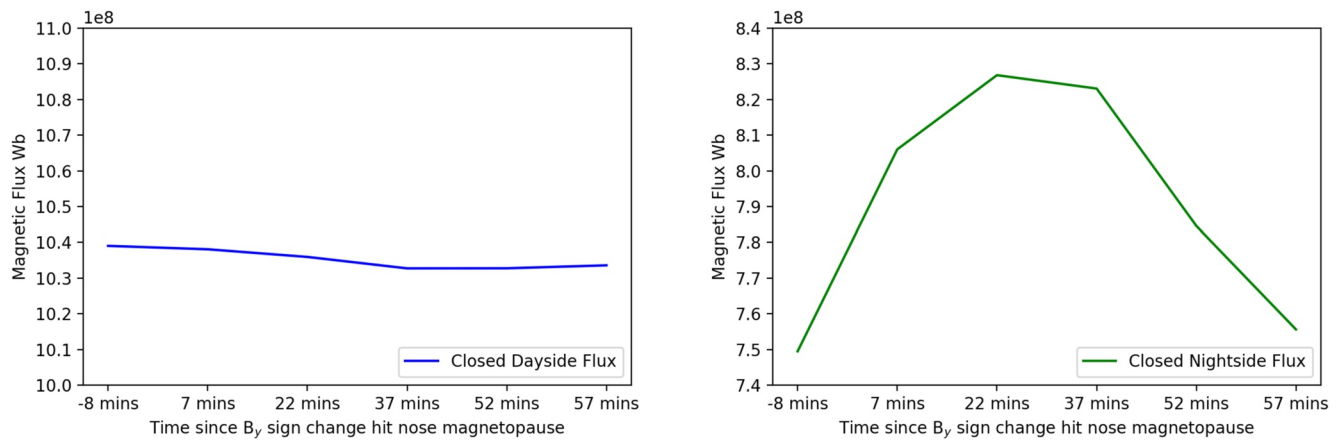


**Figure 3.** The total dayside and nightside closed magnetic flux in the  $X$ – $Y$  plane at  $Z = 0R_E$  GSM. The times correspond to those detailed in Figure 1 and the area has been taken as that shown in the central column of Figure 2. We define here dayside as any point for which  $X \geq 0R_E$  and nightside as any point which has coordinates of  $X < 0R_E$ .

of the magnetic field that is normal to the plane by the area of the cell, and sum the contributions from all cells which contain closed field lines. At each timestamp, we measure the amount of closed magnetic flux on both the dayside ( $X \geq 0R_E$  GSM) and nightside ( $X < 0R_E$  GSM). The results of this can be seen in Figure 3 with the left graph showing the total closed flux on the dayside and the right-hand side showing the total closed magnetic flux on the nightside.

The total amount of closed flux on the dayside stays nearly constant throughout the simulation. However, on the nightside, we observe a significant increase in closed flux over the first 30 min after the IMF  $B_y$  sign change was introduced into the simulation. The peak in total nightside magnetic flux occurs at  $t = 22$  min rather than  $t = 37$  min (which is the time at which the closed wedge in the magnetotail extends to its maximum length downtail). We suggest that this could be due to the initiation of dual lobe reconnection (signified by a backwards “C” shape in the field lines as previously discussed), as it appears to be the dominant process causing the erosion of the wedge with time, first appearing at  $t = 37$  min in Figure 1d. The amount of closed flux then decreases with time, as expected from the initial observations in Figure 1 where we observed the stripping of the wedge in the later stages of the simulation (Figures 1e and 1f).

The observation of an increase in nightside magnetic flux, while the total dayside magnetic flux remained constant, leads us to believe that there could be some form of magnetotail reconnection occurring within the simulation. To look for signs of reconnection, we use a similar technique to that described by Laitinen et al. (2006) in which the simulation is searched for regions which contain four types of magnetic field line topologies at adjacent points.

We choose to define a volume of width  $16R_E$ ,  $11R_E$ , and  $11R_E$  in the  $X$ ,  $Y$ , and  $Z$  directions, respectively, which contains closed, interplanetary, and two oppositely connected open field lines. This volume is centered on the most tailward closed field line. Figure 4 shows the global perspective of the configuration of the magnetic field lines around the 3D region that contains all four topologies at the time of the initial growth of the wedge. The panels shown correspond to times of  $t = 2$  min (Figures 4a–4d) and  $t = 12$  min (Figures 4e and 4f) after the IMF  $B_y$  sign change hit the nose of the magnetosphere. These times are chosen to straddle the  $t = 7$  min timestamp shown in Figures 1b and 2, as this was the time at which the wedge appeared to grow, resulting in an increase in the length of the closed region of the Earth’s magnetotail. The top two panels (a) and (b) show a selected subset of the field lines within the simulation at  $t = 2$  min in the GSM  $X$ – $Z$  and  $Y$ – $Z$  planes, respectively, and panels (c) and (d) show a more densely populated  $1R_E$  resolution view at the same time. Panels (e) and (f) have the same resolution as the figures shown in (c) and (d) but show  $t = 12$  min. The topology of the field lines within each plot is indicated by color, where magenta signifies the field line is closed, green and orange are open field lines connected to the Northern and Southern Hemispheres, respectively, and IMF field lines are shown in blue.

Figure 4a shows the configuration of the magnetotail at  $t = 2$  min. At this time, a small closed field line region extends down to  $\sim 40R_E$  downtail, similar to the length of the closed magnetotail 5 min later at 7 min, shown in both Figures 1b and 2. Just tailward of this closed field line region, there are two regions of open field lines

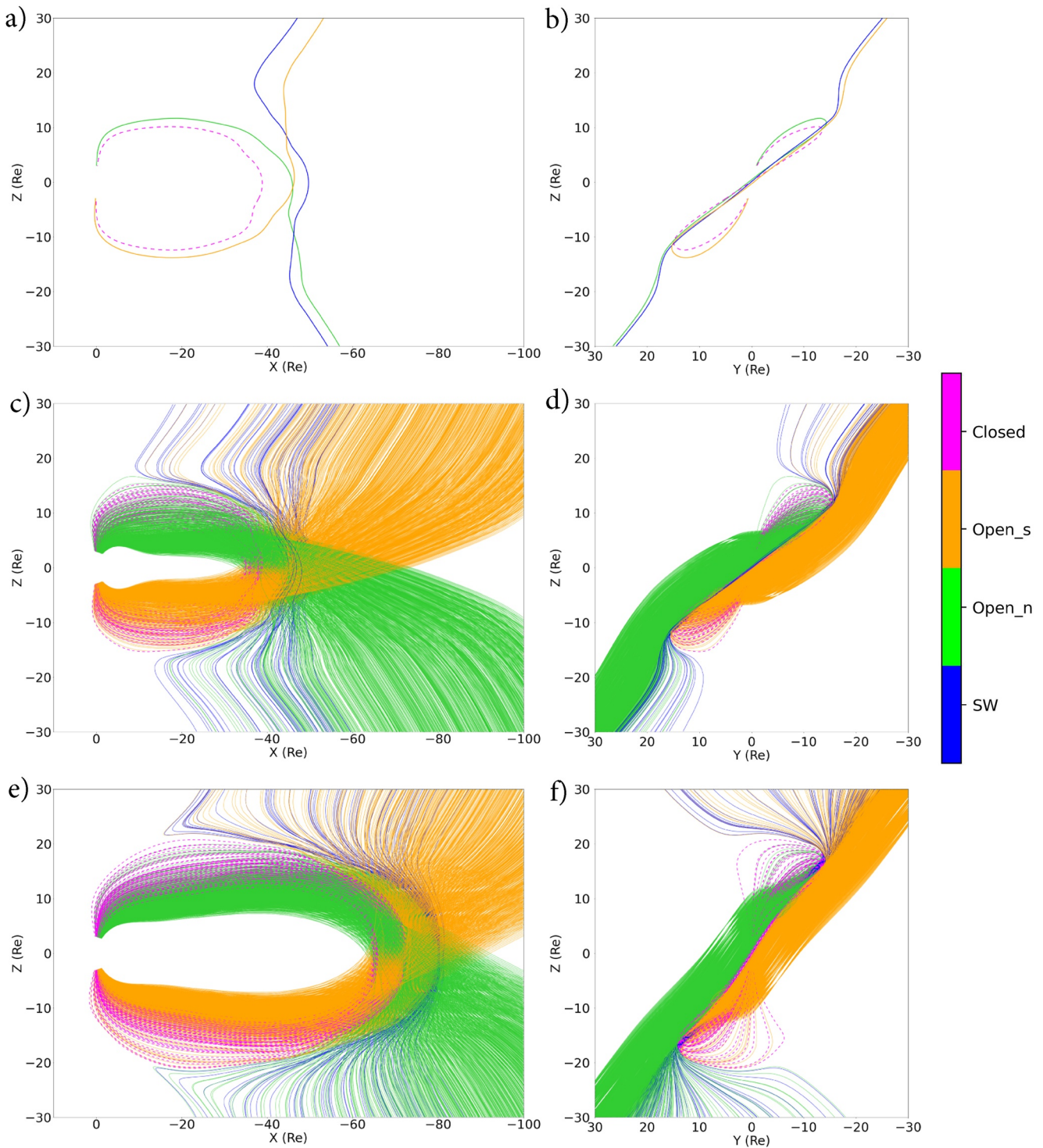


**Figure 4.** Field line traces of the region which contained all four topologies within the magnetotail 2 min (a–d) and 12 min (e, f) after the IMF  $B_y$  sign change had hit the nose of the dayside magnetopause boundary. Both timestamps are shown in two perspectives, the X–Z (left) and Y–Z planes (right). Field line topologies are indicated by colors where magenta field lines are representing closed field lines, blue are solar wind, and green and orange are open field lines connected to the Northern and Southern Hemispheres, respectively. Closed field lines are also distinguishable by a dashed line style.

connected to alternate hemispheres (seen in green and orange). An interplanetary field line (seen in blue) is located at distances further down the tail (for low  $Z$  regions), replicating typical tail reconnection configurations.

Open field lines can be seen to cross the  $X$  axis in Figure 4a and leave the simulation domain at opposite sides of the simulation box. Northern Hemispheric open field lines (green) leave the simulation box at negative  $Z$ -values, while Southern Hemispheric open field lines (orange) leave the simulation at positive  $Z$ -values, resembling an “alpha-like” shape. This is similar to the configurations discussed by Nishida et al. (1998), Park et al. (2015), Fuselier et al. (2018), and Li et al. (2021, 2022). This result arises from the fact that the field lines are directed northward for the entirety of the simulation, including the initialization phase. Therefore, the open (green and orange) and solar wind field lines (blue) downtail prior to the IMF  $B_y$  sign change are configured based on the dipole having been stripped away by high-latitude reconnection resulting from the interaction between the dipole and the incoming northward IMF. Figure 4b shows the same field lines at the same timestamp but from a different perspective, the  $Y$ - $Z$  plane. From this figure, we can see that the location of the two populations of open field lines (green and orange) cross from dawn to dusk at  $Y = Z = 0$ .

Looking at the magnetotail at the same time, but with increased field line density (shown in Figure 4c), we can see that the two regions of open field lines populate a large region of the magnetotail. Interestingly, some of the interplanetary field lines shown in blue, at high  $Z$ -values, are located earthward of the majority of the open field line ends. This complex configuration is comparable to the results from the northward IMF OpenGGCM simulation run discussed by Li et al. (2021) (shown in their Figure 10c1).

Figure 4d allows us to analyze the mid-tail region in more detail and reveals that the two open field line regions align along the same clock angle (orientated at a  $-45^\circ$  clock angle, aligned with the initial IMF conditions). There is additionally a region of IMF field lines which appears in this projection to be sandwiched between these two open field line regions. The high-latitude ends of these field lines can be seen to be the most affected by the incoming  $B_y$  sign change as they are twisted clockwise compared with the majority of the open field line regions in both the Northern and Southern Hemispheres. Despite this twist, there are a small number of open field lines which can be seen to be distributed between the downtail interplanetary field line region, as also seen in the previous panel (c).

Looking at the simulation 10 min later in Figure 4e, at  $t = 12$  min since the IMF  $B_y$  sign change hit the nose of the magnetopause, we observe that there is a significant increase in the length of the closed field line region within the magnetotail (indicated by the magenta field lines) as it now extends to  $\sim 70R_E$  downtail. Not only has the wedge increased in length, but it has also increased in height ( $Z$ -direction), as observed in Figure 2 as the wedge can be seen to reach to  $\sim Z = \pm 20R_E$ . Again looking along the  $X$  axis, we have the configuration of more earthward closed field lines followed by a mid- $X$  region where the open field lines appear to intersect, ending with a more tailward solar wind region, indicating that there is possibly a region of reconnection here (this configuration can also be observed in the 2D topological traces in Figure 2 at  $Z = 0$  as discussed above). Interestingly, looking at the  $Y$ - $Z$  plane in Figure 4f, we can see that both open and IMF field lines have been further rotated from the original negative clock angle, to more positive clock angles, presumably as a result of the penetration of the incoming positive  $B_y$  component into the magnetotail. We also note that the region of open field lines that appear interspersed within the interplanetary field line region have also undergone some rotation from the original clock angle.

In order to confirm the presence of reconnection within the magnetotail, it can be useful to use secondary plasma parameters, such as the flow velocity (Laitinen et al., 2006). Figures 5a and 5b show the  $X$ -component of the plasma velocity just before (at  $t = -8$  min) and just after (at  $t = 7$  min) the IMF  $B_y$  sign change had hit the nose of the magnetopause. We see little difference between these two states and there is no significant flow in the mid-tail and distant tail region to suggest that there is any reconnection region at larger distances downtail. At  $t = 22$  min (Figure 5c), a small region of slower tailward flow appears between  $X = -60R_E$  and  $X = -80R_E$ . This slow region of flow grows along the  $X$  axis and increases in width slightly along the  $Y$  axis. At  $t = 37$  min (Figure 5d), it extends between  $X = -40R_E$  and  $X = -100R_E$  and has a width between  $X \sim \pm 10R_E$ . We can compare this to the topological plots in the same plane in Figure 2 and can see that at  $t = 37$  min, the region of slow ( $\sim 50$  km/s) tailward plasma velocity overlaps with the region encompassing the closed wedge. This stagnated flow therefore has similarities to the properties of the “trapped wedge” discussed by Milan et al. (2005), whereby the closed field line structure straddles the noon–midnight meridian and is stuck due to the prohibited return flow around either the dawn or the dusk sides. At  $t = 52$  min (in Figure 5e), a region of fast tailward flow ( $\sim 500$  km/s) is situated

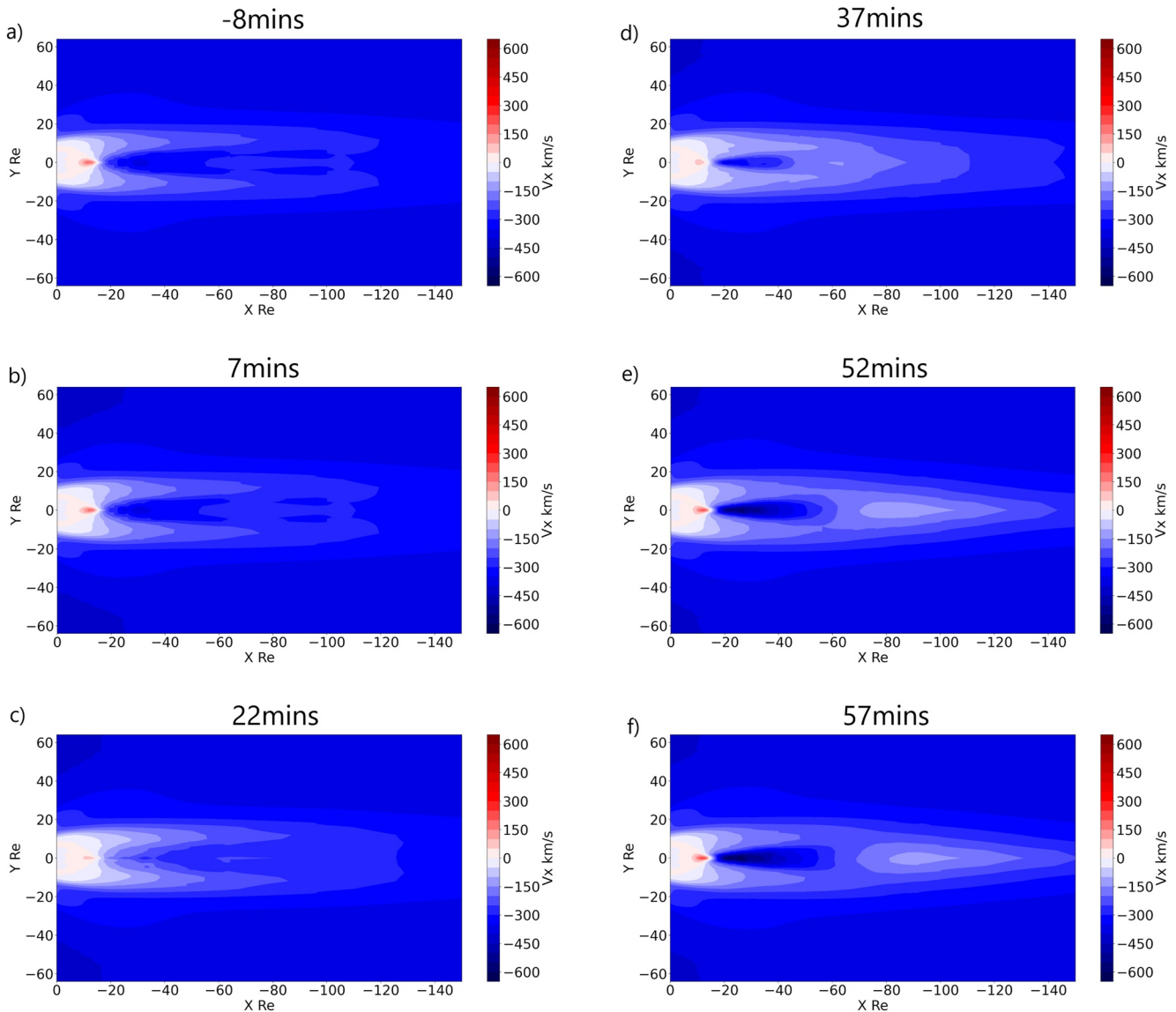


**Figure 5.** Plasma flow velocity  $x$ -component contours in the  $X$ - $Y$  plane for each of the times shown in Figure 1. These contours have been calculated from grid values at  $0.25R_E$  resolution.

earthward of the slower region, between  $X = -20R_E$  and  $X = -50R_E$ . This coincides with the regions at which the interplanetary field lines appear in the near-Earth tail region, which thread the inner wedge structure (indicated by a white arrow in Figures 1e and 2 at  $Z = 0$ ,  $t = 52$  min).

We also observed a similar distribution in the  $X$ - $Z$  plane, as no earthward flows were observed throughout the duration of the simulation (shown in Appendix A in Figure A2). The only significant difference between the two planes was the location of the slower tailward plasma flows, as in the  $X$ - $Z$  plane, which was no longer aligned along the central  $Y = 0/Z = 0R_E$  axis but had two distinct regions which formed at higher  $|Z|$  values (between 5 and  $15R_E$ ). Overall, Figure 5 shows significant tailward flow within the magnetotail but no signatures of earthward flow. This is contrary to the features observed by Li et al. (2021) in their simulation run of northward IMF with OpenGGCM, where for short periods of the order of minutes, earthward flows were observed associated with reconnection. It should be noted that significant earthward flow bursts were only observed for one out of the two models used within the Li et al. (2021) study, despite the same input of solar wind parameters. A more direct comparison of the variation in model outputs is beyond the scope of this study; however, it is further addressed by Honkonen et al. (2013).

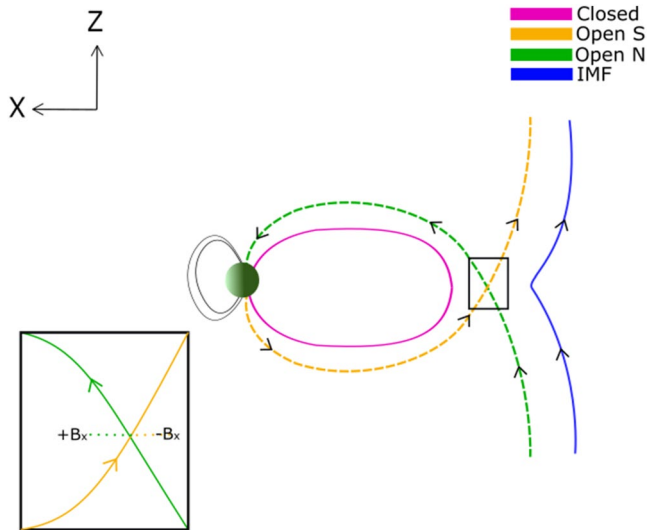


**Figure 6.** A schematic showing the proposed magnetotail reconnection processes observed in this simulation run in 2D as if viewed from the dusk side looking at the  $X$ – $Z$  plane. The colors correspond to different topologies, with magenta representing closed field lines, green and orange representing open field lines connected to the Northern and Southern Hemisphere, respectively, and blue lines representing interplanetary field lines. Dashed lines are representing configurations prior to reconnection and solid lines represent post reconnection field lines. Arrows indicate the direction of the magnetic field. The expected configuration of magnetotail reconnection during northward IMF conditions with regions of two open field lines with the same  $B_z$  components but opposite  $B_x$  components of the magnetic field. Resulting in the production of closed flux in the magnetotail and a single interplanetary field line directed northward.

To summarize, the observations we have presented in Figures 1–5 show the formation of dawn–dusk lobes (commonly associated with strong IMF  $B_y$  conditions during simulations of northward IMF). We have located regions within the simulation that show signatures associated with reconnection, in conjunction with a measured increase in the total nightside magnetic flux within the magnetotail. This is measured at the same time as an increase in length and width of the wedge of closed flux, all of which are indicative and consistent with a period of reconnection occurring in the magnetotail during the simulated period of northward IMF (with an IMF  $B_y$  sign change). Although we do not observe any earthward flows within the magnetotail, the presence of reconnection is supported by the observations of slower tailward flow regions, aligning with the wedge of closed flux that builds up within the magnetotail, consistent with the idea of the “wedge” of closed flux “stagnating” in the tail as proposed by Milan et al. (2005).

## 5. Discussion

In this paper, we have reproduced the results and extended the analysis of KJ04, who presented simulations of northward IMF dynamics using the GUMICS-4 MHD code. The features highlighted above were interpreted by KJ04 as a consequence of the change in the twist of the magnetotail, resulting in a change of mapping of field lines from the far-tail to the ionosphere, and/or a relocation of the magnetopause reconnection site. Both of these processes were argued to occur as a result of a change in the IMF orientation that was introduced into the simulation. As discussed above, both aspects of this interpretation present theoretical difficulties which have motivated our reexamination.

One process that has been argued to introduce closed field lines into the magnetotail is the process of dual lobe reconnection, which adds new closed field lines to the dayside magnetosphere, followed by a period of reverse

convection which convects them into the magnetotail (Imber et al., 2006). Indeed, we have discussed above the observations of signatures of dual lobe reconnection both early on in the initial stages of the initialization of the simulation, leaving kinked interplanetary field lines in the mid-tail (Section 4.1 and Figure 1a), and also later toward the end of the simulation, during the end of the lifetime of the closed wedge within the magnetotail, which we argued contributed to its erosion (Section 4.2 and Figures 1e and 1f). We therefore considered whether the process of dual lobe reconnection could induce a wedge structure to form in the magnetotail, by expansion of the preexisting closed field line region (i.e., the plasma sheet) in the tail. However, we argue that this is not the case here for at least two reasons. First, we measure no significant changes in the total dayside closed flux throughout the entirety of the simulation run (as shown in Figure 3), indicating that there is no closure (or opening) of field lines on the dayside and hence the nightside magnetotail is not being replenished by reverse convection from the dayside population (Dungey, 1963). Second, the fact that we measure an increase in total closed flux within the magnetotail which corresponds to the growth of the closed region downtail (without a change in the total closed flux on the dayside) strongly indicates that there is tail reconnection occurring within the magnetotail. The topological field line configurations also indicate the four-point conjunction topology commonly associated with magnetotail reconnection.

Given the observational evidence of magnetotail reconnection presented above, we interpret the formation of the nightside closed field line “wedge” as a consequence of magnetic reconnection in the magnetotail. Our interpretation is summarized by the schematic in Figure 6, which shows the expected configuration of the magnetotail as a result of magnetotail reconnection at low latitude between two open field lines connected to opposite hemispheres. The two open field lines are both northward-directed but have opposite  $B_x$  components which, we argue, allows component reconnection to occur between them. We have observed that the  $B_y$  sign change penetrates into the magnetotail, creating a rotation in both the open magnetic field lines (lobes). We suggest that this rotation results in the two regions of open field lines (connecting to opposite hemispheres) being brought into contact

with each other and reconnecting at a point close to the  $X$  axis, where these field lines cross (see also Figure 4). This results in the formation of a closed field line and a single interplanetary field line downtail (solid magenta and solid blue, respectively, in Figure 6). We observed this kind of configuration within the field line traces in Figure 4 which coincided with the start of the growth of this wedge structure. During this process, there is no expected change to the amount of closed flux on the dayside, but there would be an increase in closed flux measured on the nightside, both of which were observed within this simulation (see Figure 3). This configuration has some similarities with the mechanism proposed by Milan et al. (2005), in that closed field lines are formed in the magnetotail by magnetotail reconnection during a period of northward IMF, and this results in the buildup of an azimuthally narrow “wedge” of closed flux in the magnetotail which extends to high latitudes, as seen observationally by Fear et al. (2014), Fryer et al. (2021), and Coxon et al. (2021). However, the configuration we observe in this simulation differs from that proposed by Milan et al. (2005) in one major respect, which is that the instigation of magnetotail reconnection appears to be inherently linked to the alpha-like configuration of the magnetotail. It is this configuration that means that a rotation in the tail (arising from a change in the sign of the IMF  $B_y$  component) can bring the Northern and Southern Hemisphere open field lines into contact, allowing reconnection to occur.

The “alpha-like” magnetotail configuration arises due to reconnection between the IMF and closed magnetospheric field lines during the initialization phase (as the simulation is initialized with a dipole field). Observationally, it is not entirely clear whether the “alpha-like” configuration is representative of the real magnetotail during periods of northward IMF, and indeed the real magnetotail configuration is likely to depend on conditions such as the length of time for which the IMF has been northward, how strongly northward the clock angle has been, and in particular, how long it takes newly reconnected northward IMF field lines to move into the main body of the magnetotail. On the one hand, newly reconnected northward IMF field lines do adopt a configuration that is similar to that in Figure 6, regardless of whether the magnetospheric field lines they reconnect with are open or closed prior beforehand—see configurations sketched originally by Cowley (1981, 1983) and invoked by several subsequent authors (Crooker, 1992; Fear et al., 2015; Fuselier et al., 2018). Therefore, in some senses, the configuration could be viewed as realistic. However, the real-life IMF varies between periods of northward and southward IMF, and so the starting point (when the IMF first turns northward) is a “southward-IMF” magnetotail, and there will be significant quantities of initial magnetotail lobe flux that must be displaced or removed before the field lines that are added to the magnetotail lobes during the northward IMF period begin to dominate the magnetotail. Therefore, another possibility is that the “alpha-like” field lines become much more stretched downtail by the time they reach the central regions of the tail. If that is the case, our simulation results are still representative of TPAs in that we observe a closed field line that is formed by nightside reconnection closing lobe flux, but the precise trigger of the nightside reconnection process might not be realistic. We therefore do not draw a conclusion on how representative the observed pre-TPA magnetotail configuration is of the “real” northward IMF magnetotail, but note the occurrence of the alpha-like configuration and reconnection in the GUMICS simulation with interest. The structure and shape of lobe field lines under various northward IMF conditions would be an interesting future avenue of research, both observationally and in simulations.

Moving on to comparisons with other recent results, there are some similarities between the features of our simulation run and the results of Li et al. (2021), but there are also some interesting differences. Initially, one might expect the closed wedge to contract and be associated with strong earthward flows, similar to those traditionally associated with northward IMF substorm conditions as discussed by Lee et al. (2010), Miyashita et al. (2011), Park et al. (2015), Li et al. (2021), and references therein. However, in our simulation, it is clear (from the middle panels in Figure 2) that the wedge increased in length toward more negative  $X$ -values rather than forming and contracting earthward. This configuration is further supported by the topological field line traces (e.g., at  $t = 2$  in Figure 4a) where the wedge can be seen surrounded by open field lines more tailward and closed field lines more earthward. This forms a complex topology which means that the closed field line region appears to be intertwined between the remaining open field lines which have not yet undergone reconnection and the pre-existing smaller closed region which was present at the start of the simulation at lower latitudes located more earthward (comparable to a typical plasma sheet like configuration). Therefore, it appears that the closed field line region cannot contract, which explains why no strong earthward flows are observed. Another factor that may contribute to the lack of strong Earthward flows is that the reconnection occurs between field lines that meet at an angle to each other, rather than being nearly antiparallel as is the textbook substorm/plasmoid reconnection scenario.



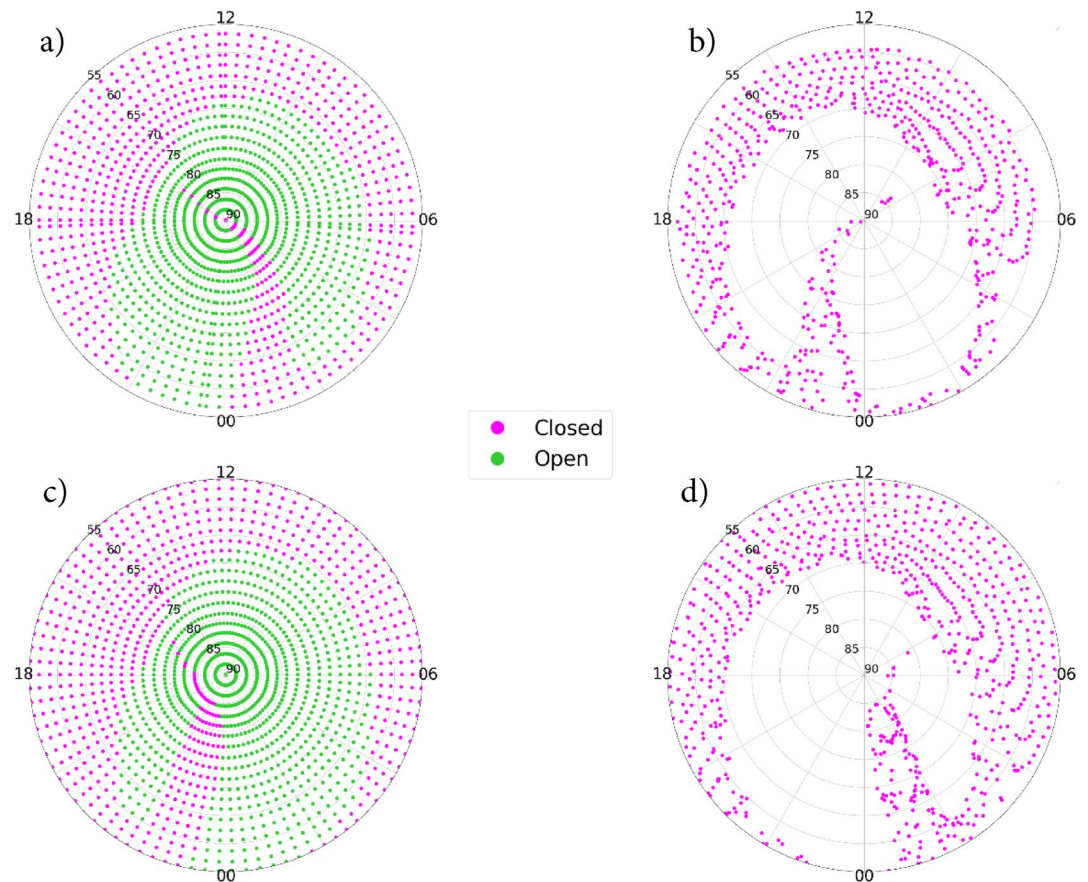
This means that a smaller fraction of the total magnetic flux participates in the reconnection process, resulting in weaker exhausts from the reconnection region.

Figure 5d shows that a larger region of slow plasma is present at the locations in which the wedge has formed. A similar field line configuration was observed in the OpenGGCM run presented by Li et al. (2021) (their Figure 10c1). However, we observe a significant difference between the lifetime of the wedge structures within this simulation and the results discussed by Li et al. (2021). Li et al. (2021) observed earthward flows starting 1 hr after the start of northward IMF conditions, with the last burst occurring 4 hr after the introduction of northward IMF. This indicates that the closed field line region observed within their study has a longer lifetime, on the order of hours, compared with our simulation, as the wedge in our simulation erodes within an hour of its first growth signatures (Figure 1). This is likely to be a result of the difference in solar wind conditions fed into the simulation (as Li et al. [2021] used real event data in their study), but inherent differences in the models (such as resolution or type of solver) could also play a part in the discrepancies observed between these different models (Hosokawa et al., 2020).

A follow-up study by Li et al. (2022) showed evidence of dawn–dusk lobe regions during observed and simulated northward IMF conditions. ARTEMIS data and the OpenGGCM global MHD model were used to study the conditions of northward IMF events and the resulting magnetotail structures. Their results were consistent with the topological features observed within their previous study Li et al. (2021), as well as the alpha-like configurations shown in this study. Like KJ04, Li et al. (2022) interpreted their results as consistent with the Chang et al. (1998) model and described their formation of a closed field line region as being due to field lines that were trapped between new and old lobe regions (shown in their Figure 12). We previously discussed the physical limitations of the model proposed by Chang et al. (1998); we would suggest that a modified magnetotail reconnection mechanism such as that described by Milan et al. (2005) would be more consistent with the results of Li et al. (2021, 2022), which are in turn consistent with our results. Interestingly, very similar dawn–dusk open lobe populations and resulting closed wedge structures that form in the high latitudes are present in simulations using real events (such as those discussed by Li et al. [2021, 2022]) and artificial simulated conditions (as discussed by Kullen and Janhunen (2004) and this study). This may indicate that these northward IMF phenomena are a result of macroscopic IMF characteristics, and not microscopic changes in preceding solar wind conditions.

The topological plots in Figure 2, with particular focus on the closed regions in the large magnitude  $Z$  planes, showed that the wedge had a conjugate-like nature where it forms on alternate sides of the equatorial plane, comparable to the structure described in theory by Milan et al. (2005) and direct observations by Obara et al. (1988), Huang et al. (1989), Carter et al. (2017), Xing et al. (2018), Fryer et al. (2021), and references therein. If we trace the field lines threading a spherical shell at the ionospheric boundary of the magnetospheric simulation, we can identify the topologies that trace down to the polar cap, as shown in Figure 7. We trace magnetic field lines in the northern polar cap between  $55^\circ$  and  $90^\circ$  latitude with a resolution of  $2^\circ$  latitude and 0–24 MLT with  $\sim 0.25$  MLT resolution, to the southern ionospheric boundary. We show the configuration of the polar cap at  $t = 22$  min and  $t = 37$  min (the same times as shown in previous simulation figures), which captures the main observed motion of the arc-like feature observed within the polar cap. There is a large portion of the lower latitude region (at both times) dominated by closed field lines (representative of the auroral oval and mapping to the plasma sheet region), with the dayside oval boundary extending to higher latitudes than the nightside, as expected. However, we can observe a high-latitude protrusion of the closed field line region on the nightside, into the open polar cap. As previously discussed (and shown in Figure 2), we initially see the wedge form on the dawn side in the Northern Hemisphere, which corresponds to a TPA-like structure on the dawn side of the northern polar cap (seen in Figure 7a) and a conjugate arc structure is also seen in the Southern Hemisphere (Figure 7b) on the dusk side. With these ionospheric traces, we can observe the same movement duskward/dawnward in the Northern/Southern Hemispheres, respectively (Figures 7c and 7d), as previously observed in Figure 2. Therefore, the development of this large closed wedge that formed during this northward IMF simulation resembles the development of the global structure discussed by Milan et al. (2005).

We can compare the motion and location of the arc-like formation within this simulation to previous observational studies. We observe that the TPA-like feature forms in the initial stages of the simulation on the dawn side (when viewed from the Northern Hemisphere) and then progresses to move toward the noon–midnight meridian and stagnates on the dusk side. This motion is demonstrated well in Figure 2 whereby the closed field line region forms at negative  $Y$  values within the positive high-latitude plane ( $Z = 15R_E$ ), and



**Figure 7.** Footprints of field lines at  $t = 22$  and  $t = 37$  min since the interplanetary magnetic field (IMF)  $B_y$  sign change hit the nose of the magnetopause. The points have been traced from the Northern Hemisphere at a  $3.7R_E$  radius with a spherical grid between  $55^\circ$  and  $90^\circ$  MLAT with a resolution of  $2^\circ$  MLAT, and 0–24 MLT with  $\sim 0.25$  hr resolution. The topologies of the field lines can be seen in the same color scheme as Figure 4 where closed field lines can be seen in magenta and open field lines in green. (a, c) The Northern Hemispheric traces for  $t = 22$  min and  $t = 37$  min, respectively. The Southern Hemispheric footprints seen on the right in panels (b) and (d) have been traced from the Northern Hemispheric footprints only, and hence only contain points that are closed. All Southern Hemispheric traces have been plot as if viewing through the Earth from the Northern Hemisphere, with dawn to the right.

then progresses to positive  $Y$  values with time, or Figure 7 where we observe the protrusion of closed field lines initially on the dawn side and later toward dusk (in the Northern Hemisphere). The opposite motion is observed for the Southern Hemisphere (or negative  $Z$  planes) and hence consistent with characteristics of conjugate arcs.

Previous statistical studies, such as those by Gussenhoven (1982), Fear and Milan (2012a), and Kullen et al. (2015), have shown that there is a dependence between the local time at which TPAs form and the IMF  $B_y$  component. Fear and Milan (2012a) explicitly showed that there was an improved correlation between the IMF  $B_y$  component and the location of the arc when the IMF conditions were averaged between 3 and 4 hr prior to the arc's emergence while Kullen et al. (2015) observed a peak in the correlation with 1–2 hr lag. Both studies found that if the IMF  $B_y$  component was negative within their respective average windows prior to the observations of an arc, the arc was most likely to form post-midnight in the Northern Hemisphere (and pre-midnight in the Southern Hemisphere). Hence, as this run has been initialized with 2 hr of negative IMF  $B_y$  conditions, before the IMF rotation, the formation location of this arc on the dawnside in the Northern Hemisphere (and dusk side in the south) agrees with the statistical behavior observed by Fear and Milan (2012a).

## 6. Conclusion

The results found from this simulation suggest that there is evidence for reconnection in the magnetotail, resulting in an increased amount of closed flux measured on the nightside. We interpret this as a buildup of a “wedge” of closed flux in the magnetotail, which is the magnetospheric counterpart of a TPA. The “wedge” and region of closed field lines traced to the ionosphere are similar in many respects to the interpretation inferred from magnetospheric and ionospheric observations of TPAs and corresponding magnetospheric structure (Coxon et al., 2021; Fear & Milan, 2012a, 2012b; Fear et al., 2014; Fryer et al., 2021; Milan et al., 2005). Our interpretation differs from that of Kullen and Janhunen (2004), who argued that the observations were due to a combination of two mechanisms—one in which the TPA arises due to the way the distant plasma sheet was argued to map to the ionosphere when a twist is applied to the magnetotail (Kullen, 2000) and a second which interpreted a TPA-like feature as a result of a change in the location of the magnetopause reconnection site “trapping” regions of closed flux within the polar cap (Chang et al., 1998).

We do note that there is a key difference between our simulation results and observational interpretations, which is that the magnetotail reconnection occurs due to the “alpha-like” configuration of the magnetotail, which arises from the northward IMF initialization of the simulation, but bears similarities to dawn–dusk lobes which have been argued to form during northward IMF configurations by previous studies (Fuselier et al., 2018; Li et al., 2021, 2022). A consequence of this “alpha-like” configuration is that the two twisted open field line regions are brought into contact by the rotation of the magnetotail. This explains why, in this simulation, the formation of the wedge/TPA appears to be caused by the introduction of the IMF  $B_y$  sign change. If the “alpha-like” structure of the northward IMF magnetotail proves to be observationally realistic, that might indicate that a minor modification of the Milan et al. (2005) TPA model (which has been successful in explaining multiple TPA observations), could be beneficial, to account for the presence of dawn–dusk lobes that appear to be common in recent simulations.

## Appendix A: Additional Simulation Fields of View

This appendix contains two further figures which show additional fields of view within the simulation. Figure A1 shows multiple views of the 3D field line traces made at time  $t = 52$  mins within the simulation. Figure A2 shows the  $X$  component of the plasma velocity in the  $X$ – $Z$  plane within the simulation.

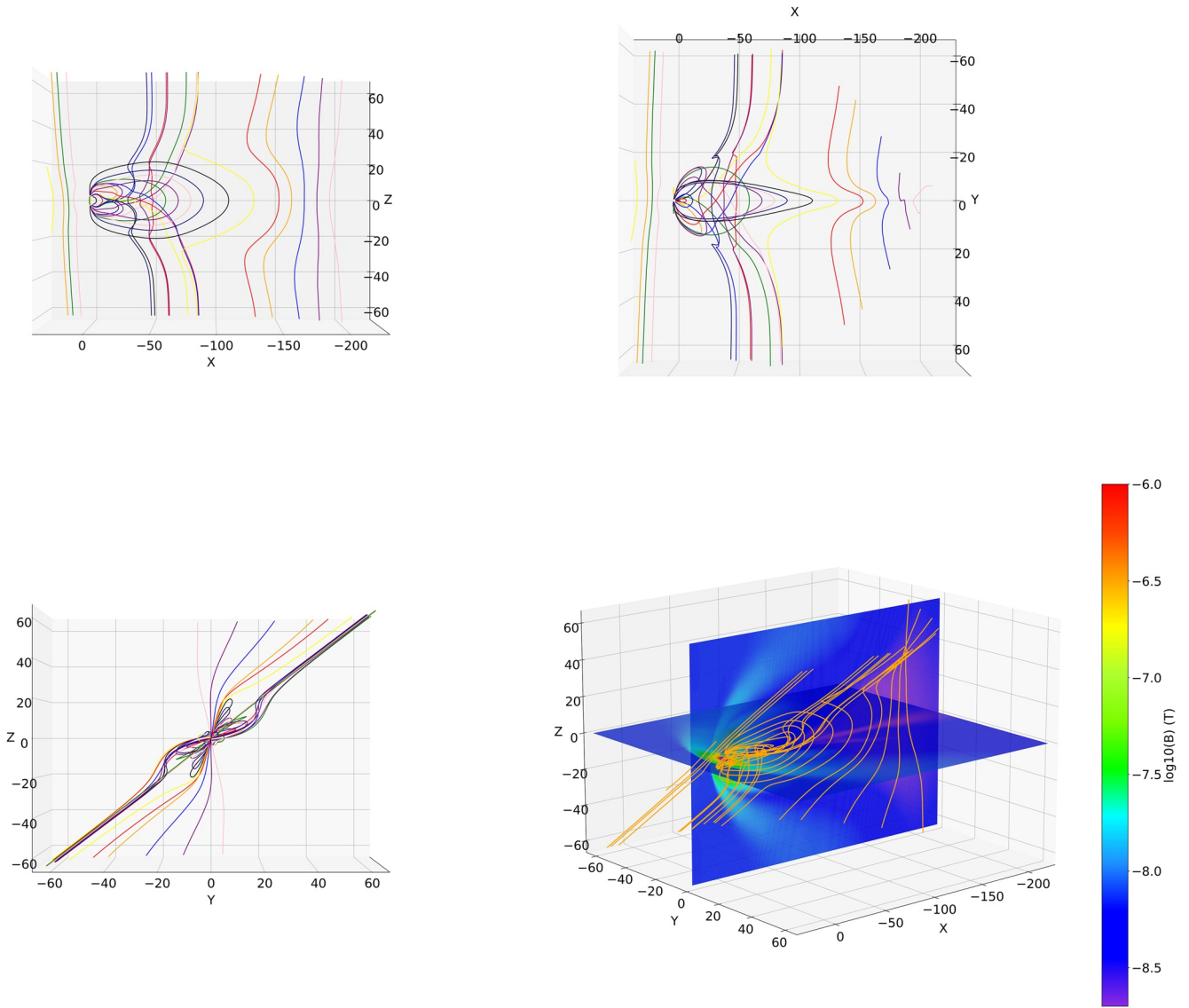


**Figure A1.** Field line traces in  $X$ - $Z$ ,  $X$ - $Y$ ,  $Z$ - $Y$ , and 3D field line trace plots for  $t = 52$  min. The bottom right figure replicates the 3D field line traces from Figure 1 at  $t = 52$  min. The 2D planes have sequential field lines traced with different colors. The black, purple, and red field lines, which have their ends leaving the simulation domain between  $X = -50$  and  $-65R_E$ , thread through the population of closed field lines (the “wedge”).

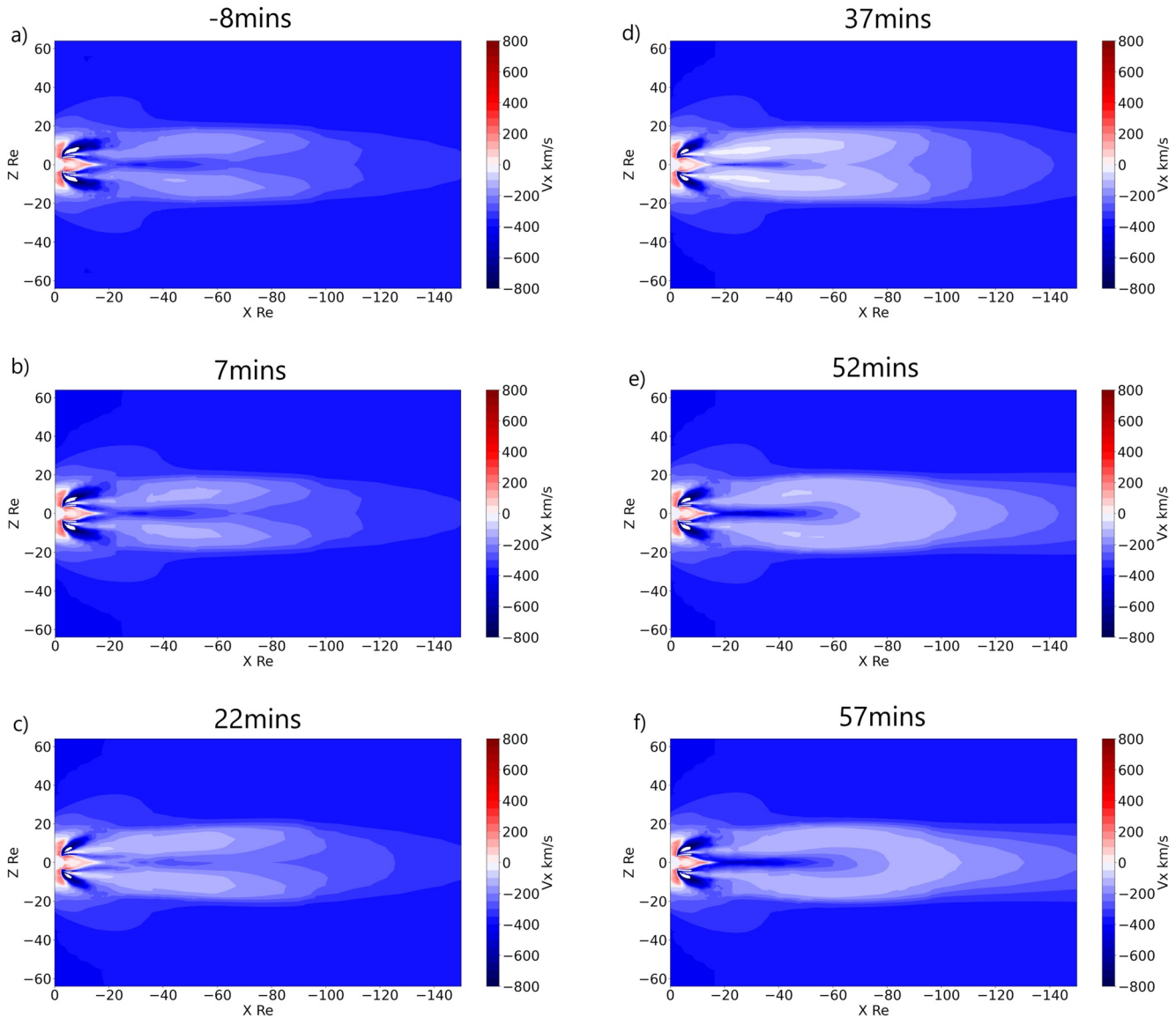


**Figure A2.** Plasma flow velocity X-component contours in the X-Z plane in the same format at Figure 5.

### Data Availability Statement

This paper uses the closed-source GUMICS-4 code. A GUMICS license was provided to the University of Southampton by the Finnish Meteorological Institute, Helsinki, Finland, to run the GUMICS-4 model locally. GUMICS-4 is also available open source at <https://ccmc.gsfc.nasa.gov/models/GUMICS~4-HC-1.11/> through the CCMC interface. All parameters that can be input into the open-source version of GUMICS are listed in Section 3 of this paper which could be used to recreate this run. (*Note:* The output of the GUMICS-CCMC code has not been verified against this output run directly with the GUMICS model).

### References

- Bower, G. E., Milan, S. E., Paxton, L. J., & Anderson, B. J. (2022). Occurrence statistics of horse collar aurora. *Journal of Geophysical Research: Space Physics*, 127, e2022JA030385. <https://doi.org/10.1029/2022JA030385>
- Browett, S. D., Fear, R. C., Grocott, A., & Milan, S. E. (2017). Timescales for the penetration of IMF  $B_y$  into the Earth's magnetotail. *Journal of Geophysical Research: Space Physics*, 122, 579–593. <https://doi.org/10.1002/2016JA023198>

### Acknowledgments

LJF is supported by the UK's Science and Technology Facilities Council (STFC) through studentship ST/T506424/1 (2279917). RCF is supported by STFC consolidated Grant ST/R000719/1. MP is supported by the Academy of Finland Grants 339327, 335554, 347795, 345701, and 336805. PAC is supported by NASA Grant 80NSSC22K0323.

- Carter, J. A., Milan, S. E., Fear, R. C., Walach, M. T., Harrison, Z. A., Paxton, L. J., & Hubert, B. (2017). Transpolar arcs observed simultaneously in both hemispheres. *Journal of Geophysical Research: Space Physics*, 122, 6107–6120. <https://doi.org/10.1002/2016JA023830>
- Chang, S. W., Scudder, J. D., Sigwarth, J. B., Frank, L. A., Maynard, N. C., Burke, W. J., et al. (1998). A comparison of a model for the theta aurora with observations from Polar, Wind, and SuperDARN. *Journal of Geophysical Research: Space Physics*, 103(A8), 17367–17390. <https://doi.org/10.1029/97JA02255>
- Cowley, S. W. H. (1981). Magnetospheric and ionospheric flow and the interplanetary magnetic field. In *The physical basis of the ionosphere in the solar-terrestrial system* (p. 14). AGARD.
- Cowley, S. W. H. (1983). Interpretation of observed relations between solar wind characteristics and effects at ionospheric altitudes. In B. Hultqvist & T. Hagfors (Eds.), *High-latitude space plasma physics* (pp. 225–249). Springer US. [https://doi.org/10.1007/978-1-4613-3652-5\\_13](https://doi.org/10.1007/978-1-4613-3652-5_13)
- Coxon, J. C., Fear, R. C., Reidy, J. A., Fryer, L. J., & Plank, J. (2021). Hot plasma in the magnetotail lobes shows characteristics consistent with closed field lines trapped in the lobes. *Journal of Geophysical Research: Space Physics*, 126, e2021JA029516. <https://doi.org/10.1029/2021JA029516>
- Craven, J. D., Murphree, J. S., Frank, L. A., & Cogger, L. L. (1991). Simultaneous optical observations of transpolar arcs in the two polar caps. *Geophysical Research Letters*, 18(12), 2297–2300. <https://doi.org/10.1029/91GL02308>
- Crooker, N. U. (1992). Reverse convection. *Journal of Geophysical Research*, 97(A12), 19363–19372. <https://doi.org/10.1029/92JA01532>
- Cumnock, J. A. (2005). High-latitude aurora during steady northward interplanetary magnetic field and changing IMF  $B_y$ . *Journal of Geophysical Research*, 110, A02304. <https://doi.org/10.1029/2004JA010867>
- Cumnock, J. A., Sharber, J. R., Heelis, R. A., Hairston, M. R., & Craven, J. D. (1997). Evolution of the global aurora during positive IMF  $B_z$  and varying IMF  $B_y$  conditions. *Journal of Geophysical Research*, 102(A8), 17489–17498. <https://doi.org/10.1029/97JA01182>
- Dungey, J. W. (1963). The structure of the exosphere, or adventures in velocity space. *Geophysics, the Earth's Environment*. Retrieved from <https://ci.nii.ac.jp/naid/10017469554/en/>
- Fear, R. C. (2021). The northward IMF magnetosphere. In R. Maggiolo, N. André, H. Hasegawa, & D. T. Welling (Eds.), *Magnetospheres in the solar system* (Vol. 2, p. 293). <https://doi.org/10.1002/9781119815624.ch19>
- Fear, R. C., & Milan, S. E. (2012a). The IMF dependence of the local time of transpolar arcs: Implications for formation mechanism. *Journal of Geophysical Research*, 117, A03213. <https://doi.org/10.1029/2011JA017209>
- Fear, R. C., & Milan, S. E. (2012b). Ionospheric flows relating to transpolar arc formation. *Journal of Geophysical Research*, 117, A09230. <https://doi.org/10.1029/2012JA017830>
- Fear, R. C., Milan, S. E., Carter, J. A., & Maggiolo, R. (2015). The interaction between transpolar arcs and cusp spots. *Geophysical Research Letters*, 42, 9685–9693. <https://doi.org/10.1002/2015GL066194>
- Fear, R. C., Milan, S. E., Maggiolo, R., Fazakerley, A. N., Dandouras, I., & Mende, S. B. (2014). Direct observation of closed magnetic flux trapped in the high-latitude magnetosphere. *Science*, 346(6216), 1506–1510. <https://doi.org/10.1126/science.1257377>
- Fedder, J. A., Lyon, J. G., Slinker, S. P., & Mobarry, C. M. (1995). Topological structure of the magnetotail as a function of interplanetary magnetic field direction. *Journal of Geophysical Research*, 100(A3), 3613–3622. <https://doi.org/10.1029/94JA02577>
- Fedder, J. A., Slinker, S. P., Lyon, J. G., & Russell, C. T. (2002). Flux transfer events in global numerical simulations of the magnetosphere. *Journal of Geophysical Research*, 107(A5), 1048. <https://doi.org/10.1029/2001JA000025>
- Frank, L. A., Craven, J. D., Burch, J. L., & Winningham, J. D. (1982). Polar views of the Earth's aurora with Dynamics Explorer. *Geophysical Research Letters*, 9(9), 1001–1004. <https://doi.org/10.1029/GL009i009p01001>
- Frank, L. A., Craven, J. D., Gurnett, D. A., Shawhan, S. D., Weimer, D. R., Burch, J. L., et al. (1986). The theta aurora. *Journal of Geophysical Research*, 91(A3), 3177–3224. <https://doi.org/10.1029/JA091iA03p03177>
- Fryer, L. J., Fear, R. C., Coxon, J. C., & Gingell, I. L. (2021). Observations of closed magnetic flux embedded in the lobes during periods of northward IMF. *Journal of Geophysical Research: Space Physics*, 126, e2021JA029281. <https://doi.org/10.1029/2021JA029281>
- Fuselier, S. A., Dayeh, M. A., Livadiotis, G., McComas, D. J., Ogasawara, K., Valek, P., et al. (2015). Imaging the development of the cold dense plasma sheet. *Geophysical Research Letters*, 42, 7867–7873. <https://doi.org/10.1002/2015GL065716>
- Fuselier, S. A., Trattner, K. J., Petrincec, S. M., Lavraud, B., & Mukherjee, J. (2018). Nonlobe reconnection at the Earth's magnetopause for northward IMF. *Journal of Geophysical Research: Space Physics*, 123, 8275–8291. <https://doi.org/10.1029/2018JA025435>
- Gombosi, T., DeZeeuw, D., Groth, C., Powell, K., & Song, P. (1998). The length of the magnetotail for northward IMF: Results of 3D MHD simulations. *Physics of Space Plasmas*, 15, 121–128.
- Gosling, J. T., Thomsen, M. F., Bame, S. J., Elphic, R. C., & Russell, C. T. (1991). Observations of reconnection of interplanetary and lobe magnetic field lines at the high-latitude magnetopause. *Journal of Geophysical Research*, 96(A8), 14097–14106. <https://doi.org/10.1029/91JA01139>
- Gosling, J. T., Thomsen, M. F., Le, G., & Russell, C. T. (1996). Observations of magnetic reconnection at the lobe magnetopause. *Journal of Geophysical Research*, 101(A11), 24765–24774. <https://doi.org/10.1029/96JA02254>
- Grocott, A., Badman, S., Cowley, S., Yeoman, T., & Cripps, P. (2004). The influence of IMF  $B_y$  on the nature of the nightside high-latitude ionospheric flow during intervals of positive IMF  $B_z$ . *Annales Geophysicae*, 22(5), 1755–1764. <https://doi.org/10.5194/angeo-22-1755-2004>
- Grocott, A., Cowley, S. W. H., & Sigwarth, J. B. (2003). Ionospheric flow during extended intervals of northward but  $B_y$ -dominated IMF. *Annales Geophysicae*, 21(2), 509–538. <https://doi.org/10.5194/angeo-21-509-2003>
- Grocott, A., Yeoman, T. K., Milan, S. E., Amm, O., Frey, H. U., Juusola, L., et al. (2007). Multi-scale observations of magnetotail flux transport during IMF-northward non-substorm intervals. *Annales Geophysicae*, 25(7), 1709–1720. <https://doi.org/10.5194/angeo-25-1709-2007>
- Grocott, A., Yeoman, T. K., Milan, S. E., & Cowley, S. W. H. (2005). Interhemispheric observations of the ionospheric signature of tail reconnection during IMF-northward non-substorm intervals. *Annales Geophysicae*, 23(5), 1763–1770. <https://doi.org/10.5194/angeo-23-1763-2005>
- Gussenhoven, M. S. (1982). Extremely high latitude auroras. *Journal of Geophysical Research*, 87(A4), 2401–2412. <https://doi.org/10.1029/JA087iA04p02401>
- Gussenhoven, M. S., & Mullen, E. G. (1989). Simultaneous relativistic electron and auroral particle access to the polar caps during interplanetary magnetic field  $B_z$  northward: A scenario for an open field line source of auroral particles. *Journal of Geophysical Research*, 94(A12), 17121–17132. <https://doi.org/10.1029/JA094iA12p17121>
- Hardy, D. A., Burke, W. J., & Gussenhoven, M. S. (1982). DMSP optical and electron measurements in the vicinity of polar cap arcs. *Journal of Geophysical Research*, 87(A4), 2413–2430. <https://doi.org/10.1029/JA087iA04p02413>
- Hoilijoki, S., Ganse, U., Pfau-Kempf, Y., Cassak, P. A., Walsh, B. M., Hietala, H., et al. (2017). Reconnection rates and X line motion at the magnetopause: Global 2D-3V hybrid-Vlasov simulation results. *Journal of Geophysical Research: Space Physics*, 122, 2877–2888. <https://doi.org/10.1002/2016JA023709>
- Hones, J. E. W., Craven, J. D., Frank, L. A., Evans, D. S., & Newell, P. T. (1989). The horse-collar aurora: A frequent pattern of the aurora in quiet times. *Geophysical Research Letters*, 16(1), 37–40. <https://doi.org/10.1029/GL016i001p00037>

- Honkonen, I., Rastätter, L., Grocott, A., Pulkkinen, A., Palmroth, M., Raeder, J., et al. (2013). On the performance of global magnetohydrodynamic models in the Earth's magnetosphere. *Space Weather*, *11*, 313–326. <https://doi.org/10.1002/swe.20055>
- Honkonen, I., van de Kamp, M., Hoppe, T., & Kauristie, K. (2022). Over 20-year global magnetohydrodynamic simulation of Earth's magnetosphere. *Space Weather*, *20*, e2022SW003196. <https://doi.org/10.1029/2022SW003196>
- Hosokawa, K., Kullen, A., Milan, S., Reidy, J., Zou, Y., Frey, H. U., et al. (2020). Aurora in the polar cap: A review. *Space Science Reviews*, *216*(1), 15. <https://doi.org/10.1007/s11214-020-0637-3>
- Huang, C. Y., Craven, J. D., & Frank, L. A. (1989). Simultaneous observations of a theta aurora and associated magnetotail plasmas. *Journal of Geophysical Research*, *94*(A8), 10137–10143. <https://doi.org/10.1029/JA094iA08p10137>
- Huang, C. Y., Frank, L. A., Peterson, W. K., Lennartsson, W., Williams, D. J., Mitchell, D. G., et al. (1987). Filamentary structures in the magnetotail lobes. *Journal of Geophysical Research*, *92*(A3), 2349–2364. <https://doi.org/10.1029/JA092iA03p02349>
- Imber, S. M., Milan, S. E., & Hubert, B. (2006). The auroral and ionospheric flow signatures of dual lobe reconnection. *Annales Geophysicae*, *24*(11), 3115–3129. <https://doi.org/10.5194/angeo-24-3115-2006>
- Imber, S. M., Milan, S. E., & Hubert, B. (2007). Observations of significant flux closure by dual lobe reconnection. *Annales Geophysicae*, *25*(7), 1617–1627. <https://doi.org/10.5194/angeo-25-1617-2007>
- Janhunen, P., & Huuskonen, A. (1993). A numerical ionosphere–magnetosphere coupling model with variable conductivities. *Journal of Geophysical Research*, *98*(A6), 9519–9530. <https://doi.org/10.1029/92JA02973>
- Janhunen, P., Palmroth, M., Laitinen, T., Honkonen, I., Juusola, L., Fackó, G., & Pulkkinen, T. I. (2012). The GUMICS-4 global MHD magnetosphere–ionosphere coupling simulation. *Journal of Atmospheric and Solar-Terrestrial Physics*, *80*, 48–59. <https://doi.org/10.1016/j.jastp.2012.03.006>
- Kessel, R. L., Chen, S. H., Green, J. L., Fung, S. F., Boardsen, S. A., Tan, L. C., et al. (1996). Evidence of high-latitude reconnecting during northward IMF: Hawkeye observations. *Geophysical Research Letters*, *23*(5), 583–586. <https://doi.org/10.1029/95GL03083>
- Kullen, A. (2000). The connection between transpolar arcs and magnetotail rotation. *Geophysical Research Letters*, *27*(1), 73–76. <https://doi.org/10.1029/1999GL010675>
- Kullen, A., Brittnacher, M., Cumnock, J. A., & Blomberg, L. G. (2002). Solar wind dependence of the occurrence and motion of polar auroral arcs: A statistical study. *Journal of Geophysical Research*, *107*(A11), 1362. <https://doi.org/10.1029/2002JA009245>
- Kullen, A., Fear, R. C., Milan, S. E., Carter, J. A., & Karlsson, T. (2015). The statistical difference between bending arcs and regular polar arcs. *Journal of Geophysical Research: Space Physics*, *120*, 10443–10465. <https://doi.org/10.1002/2015JA021298>
- Kullen, A., & Janhunen, P. (2004). Relation of polar auroral arcs to magnetotail twisting and IMF rotation: A systematic MHD simulation study. *Annales Geophysicae*, *22*(3), 951–970. <https://doi.org/10.5194/angeo-22-951-2004>
- Laitinen, T. V., Janhunen, P., Pulkkinen, T. I., Palmroth, M., & Koskinen, H. E. J. (2006). On the characterization of magnetic reconnection in global MHD simulations. *Annales Geophysicae*, *24*(11), 3059–3069. <https://doi.org/10.5194/angeo-24-3059-2006>
- Laitinen, T. V., Pulkkinen, T. I., Palmroth, M., Janhunen, P., & Koskinen, H. E. J. (2005). The magnetotail reconnection region in a global MHD simulation. *Annales Geophysicae*, *23*(12), 3753–3764. <https://doi.org/10.5194/angeo-23-3753-2005>
- Lavraud, B., Jacquy, C., Achilli, T., Fuselier, S. A., Grigorenko, E., Phan, T. D., et al. (2018). Concomitant double ion and electron populations in the Earth's magnetopause boundary layers from double reconnection with lobe and closed field lines. *Journal of Geophysical Research: Space Physics*, *123*, 5407–5419. <https://doi.org/10.1029/2017JA025152>
- Lavraud, B., Thomsen, M. F., Lefebvre, B., Schwartz, S. J., Seki, K., Phan, T. D., et al. (2006). Evidence for newly closed magnetosheath field lines at the dayside magnetopause under northward IMF. *Journal of Geophysical Research*, *111*, A05211. <https://doi.org/10.1029/2005JA011266>
- Lavraud, B., Thomsen, M. F., Taylor, M. G. G. T., Wang, Y. L., Phan, T. D., Schwartz, S. J., et al. (2005). Characteristics of the magnetosheath electron boundary layer under northward interplanetary magnetic field: Implications for high-latitude reconnection. *Journal of Geophysical Research*, *110*, A06209. <https://doi.org/10.1029/2004JA010808>
- Lee, D. Y., Choi, K. C., Ohtani, S., Lee, J. H., Kim, K. C., Park, K. S., & Kim, K. H. (2010). Can intense substorms occur under northward IMF conditions? *Journal of Geophysical Research*, *115*, A01211. <https://doi.org/10.1029/2009JA014480>
- Li, W., Angelopoulos, V., Mieth, J., Wu, L., & Li, A. (2022). The dawn–dusk tail lobe magnetotail configuration and the formation of aurora transpolar arc. *Journal of Geophysical Research: Space Physics*, *127*, e2022JA030676. <https://doi.org/10.1029/2022JA030676>
- Li, W., Wu, L., Ge, Y., & Lü, L.-Z. (2021). Magnetotail configuration under northward IMF conditions. *Journal of Geophysical Research: Space Physics*, *126*, e2020JA028634. <https://doi.org/10.1029/2020JA028634>
- Mailyan, B., Shi, Q. Q., Kullen, A., Maggiolo, R., Zhang, Y., Fear, R. C., et al. (2015). Transpolar arc observation after solar wind entry into the high-latitude magnetosphere. *Journal of Geophysical Research: Space Physics*, *120*, 3525–3534. <https://doi.org/10.1002/2014JA020912>
- Milan, S. E., Bower, G. E., Carter, J. A., Paxton, L. J., Anderson, B. J., & Hairston, M. R. (2022). Lobe reconnection and cusp-aligned auroral arcs. *Journal of Geophysical Research: Space Physics*, *127*, e2021JA030089. <https://doi.org/10.1029/2021JA030089>
- Milan, S. E., Carter, J. A., & Hubert, B. (2020). Probing the magnetic structure of a pair of transpolar arcs with a solar wind pressure step. *Journal of Geophysical Research: Space Physics*, *125*, e2019JA027196. <https://doi.org/10.1029/2019JA027196>
- Milan, S. E., Hubert, B., & Grocott, A. (2005). Formation and motion of a transpolar arc in response to dayside and nightside reconnection. *Journal of Geophysical Research*, *110*, A01212. <https://doi.org/10.1029/2004JA010835>
- Miyashita, Y., Kamide, Y., Liou, K., Wu, C. C., Ieda, A., Nishitani, N., et al. (2011). Successive substorm expansions during a period of prolonged northward interplanetary magnetic field. *Journal of Geophysical Research*, *116*, A09221. <https://doi.org/10.1029/2011JA016719>
- Mizera, P. F., Gorney, D. J., & Evans, D. S. (1987). On the conjugacy of the aurora: High and low latitudes. *Geophysical Research Letters*, *14*(3), 190–193. <https://doi.org/10.1029/GL014i003p0190>
- Naehr, S. M., & Toffoletto, F. R. (2004). Quantitative modeling of the magnetic field configuration associated with the theta aurora. *Journal of Geophysical Research*, *109*, A07202. <https://doi.org/10.1029/2003JA010191>
- Newell, P. T., Xu, D., Meng, C.-I., & Kivelson, M. G. (1997). Dynamical polar cap: A unifying approach. *Journal of Geophysical Research*, *102*(A1), 127–140. <https://doi.org/10.1029/96JA03045>
- Nishida, A. (2000). The Earth's dynamic magnetotail. *Space Science Reviews*, *91*, 507–577. <https://doi.org/10.1023/A:1005223124330>
- Nishida, A., Mukai, T., Yamamoto, T., Kokubun, S., & Maezawa, K. (1998). A unified model of the magnetotail convection in geomagnetically quiet and active times. *Journal of Geophysical Research*, *103*(A3), 4409–4418. <https://doi.org/10.1029/97JA01617>
- Nowada, M., Fear, R. C., Grocott, A., Shi, Q.-Q., Yang, J., Zong, Q.-G., et al. (2018). Subsidence of ionospheric flows triggered by magnetotail magnetic reconnection during transpolar arc brightening. *Journal of Geophysical Research: Space Physics*, *123*, 3398–3420. <https://doi.org/10.1029/2017JA024701>
- Obara, T., Kitayama, M., Mukai, T., Kaya, N., Murphree, J. S., & Cogger, L. L. (1988). Simultaneous observations of Sun-aligned polar cap arcs in both hemispheres by Exos-C and Viking. *Geophysical Research Letters*, *15*(7), 713–716. <https://doi.org/10.1029/GL015i007p00713>

- Østgaard, N., Mende, S. B., Frey, H. U., Frank, L. A., & Sigwarth, J. B. (2003). Observations of non-conjugate theta aurora. *Geophysical Research Letters*, *30*(21), 2125. <https://doi.org/10.1029/2003GL017914>
- Palmroth, M., Janhunen, P., Germany, G., Lummerzheim, D., Liou, K., Baker, D. N., et al. (2006). Precipitation and total power consumption in the ionosphere: Global MHD simulation results compared with Polar and SNOE observations. *Annales Geophysicae*, *24*(3), 861–872. <https://doi.org/10.5194/angeo-24-861-2006>
- Park, K. S., Lee, D. Y., Ogino, T., & Lee, D. H. (2015). MHD simulations using average solar wind conditions for substorms observed under northward IMF conditions. *Journal of Geophysical Research: Space Physics*, *120*, 7672–7686. <https://doi.org/10.1002/2015JA021005>
- Parnell, C. E., & Haynes, A. L. (2010). Three-Dimensional magnetic reconnection. *Astrophysics and Space Science Proceedings*, *19*, 261–276. [https://doi.org/10.1007/978-3-642-02859-5\\_20](https://doi.org/10.1007/978-3-642-02859-5_20)
- Pontin, D. I. (2011). Three-dimensional magnetic reconnection regimes: A review. *Advances in Space Research*, *47*(9), 1508–1522. <https://doi.org/10.1016/j.asr.2010.12.022>
- Priest, E. (2016). MHD structures in three-dimensional reconnection. In W. Gonzalez, & E. Parker (Eds.), *Magnetic reconnection: Concepts and applications* (pp. 101–142). Springer International Publishing. [https://doi.org/10.1007/978-3-319-26432-5\\_3](https://doi.org/10.1007/978-3-319-26432-5_3)
- Reidy, J. A., Fear, R. C., Whiter, D. K., Lanchester, B., Kavanagh, A. J., Milan, S. E., et al. (2018). Interhemispheric survey of polar cap aurora. *Journal of Geophysical Research: Space Physics*, *123*, 7283–7306. <https://doi.org/10.1029/2017JA025153>
- Reiff, P. H., & Burch, J. L. (1985). IMF  $B_y$ -dependent plasma flow and Birkeland currents in the dayside magnetosphere: 2. A global model for northward and southward IMF. *Journal of Geophysical Research*, *90*(A2), 1595–1610. <https://doi.org/10.1029/JA090iA02p01595>
- Russell, C. T. (1972). The configuration of the magnetosphere. In E. R. Dyer (Ed.), *Critical problems of magnetospheric physics* (p. 1).
- Slinker, S. P., Fedder, J. A., McEwen, D. J., Zhang, Y., & Lyon, J. G. (2001). Polar cap study during northward interplanetary magnetic field on 19 January 1998. *Physics of Plasmas*, *8*(4), 1119–1126. <https://doi.org/10.1063/1.1355680>
- Tanaka, T., Obara, T., & Kunitake, M. (2004). Formation of the theta aurora by a transient convection during northward interplanetary magnetic field. *Journal of Geophysical Research: Space Physics*, *109*, A09201. <https://doi.org/10.1029/2003JA010271>
- Tanaka, T., Obara, T., Watanabe, M., Fujita, S., Ebihara, Y., & Kataoka, R. (2017). Formation of the Sun-aligned arc region and the void (polar slot) under the null-separator structure. *Journal of Geophysical Research: Space Physics*, *122*, 4102–4116. <https://doi.org/10.1002/2016JA023584>
- Tenfjord, P., Østgaard, N., Strangeway, R., Haaland, S., Snekvik, K., Magnus Laundal, K., et al. (2018). How the IMF  $B_y$  induces a local  $B_z$  component during northward IMF  $B_z$  and characteristic timescales. In *EGU general assembly conference abstracts* (p. 2744).
- Tsyganenko, N. A. (1989). A magnetospheric magnetic field model with a warped tail current sheet. *Planetary and Space Science*, *37*(1), 5–20. [https://doi.org/10.1016/0032-0633\(89\)90066-4](https://doi.org/10.1016/0032-0633(89)90066-4)
- Usadi, A., Kageyama, A., Watanabe, K., & Sato, T. (1993). A global simulation of the magnetosphere with a long tail: Southward and northward interplanetary magnetic field. *Journal of Geophysical Research*, *98*(A5), 7503–7518. <https://doi.org/10.1029/92JA02078>
- Walker, R. J., Ogino, T., Raeder, J., & Ashour-Abdalla, M. (1993). A global magnetohydrodynamic simulation of the magnetosphere when the interplanetary magnetic field is southward: The onset of magnetotail reconnection. *Journal of Geophysical Research*, *98*(A10), 17235–17250. <https://doi.org/10.1029/93JA01321>
- Xing, Z., Zhang, Q., Han, D., Zhang, Y., Sato, N., Zhang, S., et al. (2018). Conjugate observations of the evolution of polar cap arcs in both hemispheres. *Journal of Geophysical Research: Space Physics*, *123*, 1794–1805. <https://doi.org/10.1002/2017JA024272>
- Zhang, Q.-H., Zhang, Y.-L., Wang, C., Lockwood, M., Yang, H.-G., Tang, B.-B., et al. (2020). Multiple transpolar auroral arcs reveal insight about coupling processes in the Earth's magnetotail. *Proceedings of the National Academy of Science of the United States of America*, *117*(28), 16193–16198. <https://doi.org/10.1073/pnas.2000614117>
- Zhu, L., Valladares, C. E., Sojka, J. J., Schunk, R. W., & Crain, D. J. (1996). Model-observation comparison study of multiple polar cap arcs. *Journal of Geophysical Research*, *101*(A1), 323–334. <https://doi.org/10.1029/95JA02758>